UCRL-52315

DIRECT TIME-DOMAIN TECHNIQUES FOR TRANSIENT RADIATION AND SCATTERING

E. K. Miller

J. A. Landt

July 1, 1976

Prepared for U. S. Department of Energy
under contract No. W-7405-Eng-48

LAWRENCE
LIVERMORE
LABORATORY
University of California/Livermore

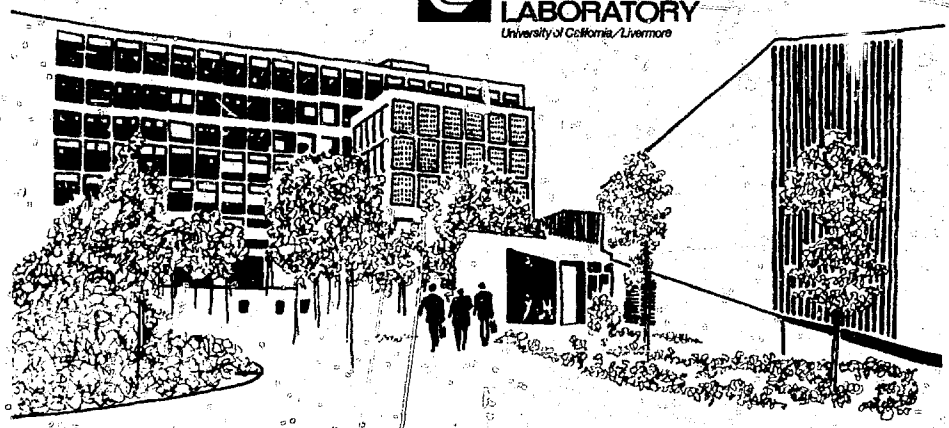

Distribution Category
UC-37

LAWRENCE LIVERMORE LABORATORY
University of California Livermore, California 94550

UCRL-52315

DIRECT TIME-DOMAIN TECHNIQUES FOR TRANSIENT RADIATION AND SCATTERING

E. K. Miller, Lawrence Livermore Laboratory
J. A. Landt, Los Alamos Scientific Laboratory

MS date: July 1, 1976

Contents

Abstract 1
Introduction 1
Definition of Terms and Overview 2
Transient Characteristics and Sampling 4
Techniques for Obtaining Time-Domain Results 5
  Analytical Techniques 5
  Numerical Techniques 6
  Singularity-Expansion Method (SEM). 8
  Asymptotic Techniques 9
  Measurement 9
Physical Aspects of Transient Analysis 9
  Some Numerical Results. 10
  Interpretation of Numerical Results 11
  Some Mathematical Relationships. 15
  The Role of Current and Charge 17
  Field Behavior 19
  Summary 20
Mathematical Aspects of Transient Analysis 21
  Direct Techniques for Obtaining Transient Results 21
  Transform Techniques for Obtaining Transient Results. 23
  Hybrid Techniques for Obtaining Transient Results. 23
    Frequency-Augmentation Technique 23
    Singularity-Expansion Method 24
  Limitations 25
Numerical Aspects of Transient Analysis 25
  Direct Techniques for Obtaining Transient Results. 26
  Transform Techniques for Obtaining Transient Results. 31
  Direct and Transform Techniques Compared. 31
  Modeling Guidelines. 34
  Degree of Applicability 36
    Configurational Factors 36
    Environmental Factors. 36
    Miscellaneous Factors. 36
  Limitations 36

Experimental Aspects of Direct Techniques 37
Time-Domain Measurements 38
The LLL Transient Facility 39
Some Representative Results 40
Applications 41
Closed Systems 42
Open Systems. 42
Applications 42
Example 43
The Linear Dipole as an Antenna 43
The Linear Dipole as a Scatterer 47
Salient Features Unique to Direct Time-Domain Analysis 51
Inherently Broadband Calculations. 51
Self-Diagnosis 53
Direct, Efficient Responses. 55
Nonlinear Capability 57
Time Gating 59
Areas of Application 60
Antenna Characteristics 60
Scatterer Characteristics 61
Transient Response. 61
EMC and RFI Analysis 61
First-Look Studies. 62
Assessment of Transient-Measurement Performance 64
Study of Modeling Errors. 65
Object-Pole Finding 67
Transient-Pulse Shaping 70
Physical Insight 72
Wire-Grid Models 74
Conclusion. 77
Acknowledgments 77
References. 78
Appendix 82

DIRECT TIME-DOMAIN TECHNIQUES FOR TRANSIENT RADIATION AND SCATTERING

Abstract

This report is a tutorial introduction to transient electromagnetics, focusing on direct time-domain techniques. We examine physical, mathematical, numerical, and experimental aspects of time-domain methods, with emphasis on wire objects excited as antennas or scatterers. Numerous computed examples illustrate the characteristics of direct time-domain procedures, especially where they may offer advantages over procedures in the more familiar frequency domain. These advantages include greater solution efficiency for many types of problems, the ability to handle nonlinearities, improved physical insight and interpretability, availability of wide-band information from a single calculation, and the possibility of isolating interactions among various parts of an object using time-range gating.

Introduction

Transient electromagnetics has interested scientists since Maxwell's equations were formulated, but our ability to obtain analytical or experimental results in this field is relatively recent. The two most important reasons for this new ability are the digital computer, which has made possible advanced computational and analytical work, and technological developments in short-pulse hardware. These two factors have significantly increased the availability of transient results for an expanding variety of electromagnetics (EM) problems.

While appreciating the academic value of understanding transient electromagnetics, one might question the practical need for, and utility of, transient solutions. But developing technology in short-pulse hardware has motivated much analytical and computational work, which in turn has demonstrated the unique contributions that transient techniques can make to a more fundamental understanding of electromagnetics in general. Thus, transient techniques are emerging as a separate branch of electromagnetics.

Current applications for transient EM include space-object identification via short-pulse radar, nuclear electromagnetic pulse (EMP) effects, and nonlinear phenomena. These and other applications represent a significant

departure from the monochromatic problems with which we may be more familiar. While some techniques used for transient or wide-band problems may not differ from those used for monochromatic problems, others may differ greatly.

This introductory, and necessarily sketchy, discussion of transient EM emphasizes engineering aspects of transients. We hope that the material will not only inform the reader about the current status of this developing technology, but also motivate him to exploit it for his own applications.

The report is organized as follows. First, we define our terms and provide an overview of the transient EM areas to be covered in this report. Next, we discuss the techniques available for realizing transient behavior in EM. Then we consider the physical, mathematical, numerical, and experimental aspects of transient analysis. Finally, we present examples and applications of transient EM. We demonstrate the variety of ways to characterize transient behavior for a given problem, as well as the variety of problem types that can be handled, and emphasize the physical interpretability of phenomena through transient analysis.

Definition of Terms and Overview

Transient electromagnetics may be broadly and qualitatively defined as all non-monochromatic EM phenomena. This report is limited to scatterers and radiators in linear, time-invariant media. Transient information can be obtained from transformed frequency-domain data or from a direct time-domain solution. This discussion focuses on the latter area, but refers to frequency-domain work to clarify the contrast between the two approaches.

More specifically, we concentrate on direct time-domain solutions for wire objects obtained from an integral-equation treatment. The narrow scope of the report allows us to treat a few topics in depth, rather than many subjects superficially. Although this tutorial report is fairly long, it covers only a small part of the developing area of transient electromagnetics. For more detail, the interested reader may consult various references (in particular, 1-5) that provide an overview of the topic.

The terms *frequency domain* and *time domain* characterize the analytical or experimental procedure used to obtain the EM response desired. A frequency-domain procedure factors out the time dependence via an $e^{i\omega t}$ multiplier. A time-domain procedure, on the other hand, treats time as an explicit independent

variable. The distinction can become blurred in pulsed continuous-wave or swept-frequency systems, but in general the frequency domain uses monochromatic or continuous-wave excitation, and the time domain uses impulsive excitation.

When seeking transient information for a linear system, then, one must decide whether to employ a frequency-domain or time-domain approach. Most earlier work in transient analysis was based on a frequency-domain formulation,[6,7] because closed-form, time-domain solutions are almost impossible to obtain. Even frequency-domain problems were difficult to solve because of the extensive computational effort required at many frequencies to evaluate a problem and transform it to the time domain. Most results from early transient analysis involved acoustic scattering from infinite cylindrical structures, because two-dimensional problems are more easily computed than three-dimensional problems.[8] More recently, Rheinstein[9] has solved three-dimensional transient EM problems (the conducting and dielectric spheres) in the frequency domain, and numerous examples resulting from EMP studies have lately been developed.[10,11]

The first time-domain approach to EM transient problems was based on physical optics to obtain the approximate backscatter-impulse response of a flat plate and spheroid.[12,13] This work was later extended to other geometries, such as the cone sphere. Subsequent direct time-domain work has concentrated on integral-equation techniques, the primary subject of this report.[14-20]

Some advantages of these direct time-domain solutions over frequency-domain treatments of transient problems are:

1) Greater solution efficiency for many types of problems.
2) More convenient handling of non-linearities.
3) Improved physical insight and interpretability.
4) Availability of wide-band information from a single calculation.
5) Opportunity to isolate interactions, using time-range gating (e.g., pulse reflection from wire ends, bends, etc.).
6) Possibility for more directly and efficiently obtaining SEM poles.

These benefits require some trade-offs, however. Foremost is the greater complexity of a time-domain code than of an equivalent frequency-domain version, with a resulting increase of difficulty in its development and use. The computing capability required can also be significantly larger.

Transient Characteristics and Sampling

A relatively recent development in EM, called the Singularity-Expansion Method (SEM),[21,22] discussed below, characterizes the transient EM response of a conducting object as a series of complex exponentials, i.e.,

$$f(t) = \sum_{\alpha=1}^{N} R_\alpha e^{s_\alpha t} \quad , \tag{1}$$

where R_α is the amplitude of each mode of complex frequency s_α. Note that, since f(t) is a real function, there are only N/2 independent terms in the summation, with the other N/2 being their complex conjugates (except for poles on the negative real axis). Thus, 4(N/2) = 2N real numbers are required to specify f(t) through the real and imaginary components of R_α and s_α. Consequently, if we know f(t), functionally or otherwise, we need 2N independent samples of it, at most, to represent it completely.

From the Shannon-Kotelnikov sampling theorem we also know that, if $s_{N/2} = \sigma_{N/2} + j\omega_{N/2}$ is the highest frequency component of f(t), then the sampling interval in time, δ, must satisfy

$$\delta \leq \frac{1}{2f_{N/2}} \quad ,$$

where $f_{N/2} = \omega_{N/2}/2\pi$. If uniform time sampling of f(t) is used, then the total observation time, T, must satisfy

$$\frac{T}{\delta} \geq 2N$$

or

$$T \geq N/f_{N/2} \quad .$$

In order to relate this result to object size, let us consider a straight wire of length L excited as a scatterer. Resonances in its response occur approximately as

$$f_\alpha \sim \alpha \frac{c}{2L} \quad ; \; \alpha = 1, 2, \ldots,$$

with c the velocity of light. Since $f_{N/2} \sim (N/2)\,(c/2L)$, we obtain

$$T \geq N/f_{N/2} = 4L/c \quad ,$$

a result that has been confirmed by numerical calculations.[23] Thus, an observation time equal to at least four transit times of the wire is required to obtain essentially all information concerning its transient response, using equally spaced time samples at intervals half the period of the maximum frequency response. Note that, if the wire is excited so that not all possible resonances are produced, then T can be made shorter, but can be no less than 2L/c, the time necessary for a wave to propagate from one end to the other and back again. Also observe that, in principle, sampling a noise-free waveform over longer observation times or using shorter intervals adds no new information to the 2N independent observations needed to specify it.

If we write the frequency-domain version of f(t) as obtained from a LaPlace transform, we can follow analagous sampling requirements. Because 2N real or N complex (phase and amplitude) samples are required to specify the transfer function, the sampling interval in frequency, δ_f, is given by

$$\begin{aligned} \delta_f &\leq f_{N/2}/N \\ &= c/4L \\ &= T^{-1} \quad . \end{aligned}$$

Techniques for Obtaining Time-Domain Results

ANALYTICAL TECHNIQUES

Unfortunately, few EM transient solutions can be expressed in closed form in terms of standard functions. In spite of that limitation, some success has been achieved for a variety of problems. Wu[24] has worked out a time-domain solution for a step-excited infinite cylindrical antenna. Chan et al.[25] have developed a closed-form solution for the diffraction of a pulsed field from an arbitrarily oriented dipole by a wedge. The latter problem belongs to a class of scattering problems for which pulse solutions take on a simpler form than do time-harmonic or frequency-domain solutions.[26] Franceschetti and

Papas[3] developed a heuristic description of the general properties of transient radiation. Even those time-domain solutions that can be given in closed form may require extensive computation to obtain numerical results. Consequently, most time-domain solutions inevitably involve substantial computer processing.

NUMERICAL TECHNIQUES

EM time-domain numerical analysis naturally proceeds from time-dependent Maxwell's equations. When we express those equations in differential form, we can solve them in terms of a finite-difference* approximation, sampling the unknown fields in both space and time. Imposed spatial boundary conditions and temporal initial values, which are also sampled in a weighted sense, lead to a system of equations which we can thus solve for the sampled values over the space considered at a sequence of time steps.

Alternatively, we can integrate Maxwell's equations, using an appropriate (usually infinite-medium) Green's function. Imposed spatial boundary conditions and temporal initial values now lead to an integral equation in which the unknowns are the sources induced on the surfaces over which the boundary conditions are applied. A sampling of these unknowns in space and time and a weighted sampling of the boundary values again lead to a system of equations for the space-time sampled values of the unknown, which is solvable as an initial-value problem.

There are some important differences between these two approaches. First, in the differential-equation formulation, the unknowns are sampled at all points within and on the boundary(ies) of the solution space. In the integral-equation formulation, on the other hand, the sampling is done only over the boundary on which the boundary conditions are applied. Thus, the integral-equation method can result in substantially fewer unknowns.

*We include any method which approximates differentials by discrete samples in the finite-difference category, e.g., the finite-element technique, uni-moment method, etc.

Second, the integral-equation treatment requires a time- and space-dependent Green's function. This function allows surface sampling to replace the volume sampling of the differential-equation formulation. For lossless, non-dispersive, homogeneous, linear, isotropic media, such a Green's function is readily obtained, but otherwise substantial complications occur that can require a volume, rather than a surface, integration. Consequently, for these more general media, an integral-equation approach may not be suitable. Nevertheless, most EM time-domain analysis to date uses the integral-equation approach.

Frequency-domain analysis is also based Maxwell's equations in differential or integral form, but for an assumed $e^{i\omega t}$ time variation. Imposed conditions on the field behavior over spatial boundaries complete the analytical formulation of the problem. A subsequent spatial sampling of the unknown, and weighted sampling of known boundary values, lead to a system of equations for the unknown sampled values.

In both the frequency domain and time domain, then, a system of equations is developed for sampled values of the unknown. The numerical solutions of these equations are substantially different, however, due to fundamental differences in their respective formulations. In the integral-equation treatment, for example, the interactions between the unknown sampled values are global in the frequency domain; i.e., the total field at a given observation point is due to the unknown sources distributed over the entire boundary. The spatial separation between the source and its field is manifested by a geometric attenuation and phase shift which are distance dependent. Consequently, all the unknown samples are mutually dependent, and must be solved simultaneously. The solutions are usually accomplished via matrix factorization or inversion.

In a time-domain integral-equation treatment, on the other hand, the interactions between unknown samples are displaced in time by an amount equal to that required for a field to propagate between them at the speed of light. This displacement (time retardation) means that a particular unknown sample value at a given point in space and time is essentially determined by the exciting field at that same space-time point and by the scattered fields there from earlier, more distant locations. Consequently, the unknown samples can be solved at any time step, provided all sample values at earlier times are already known. The time-domain problem is thus solved via time-stepping and

without matrix inversion, given the initial values of the unknown sample values.

The equations from the differential-equation formulations are treated much like those from the integral-equation approach. The frequency-domain version results in a spatial set of unknown samples, all of which can mutually interact, and which therefore require a simultaneous solution, although a given sample depends explicity on its nearest neighbors only. The time-domain approach, on the other hand, results in unknown samples whose separation produces a time retardation in their interaction, and so permits a time-stepping solution.

SINGULARITY-EXPANSION METHOD (SEM)

We normally associate transformed frequency-domain data with real frequencies; i.e., the ω in $e^{i\omega t}$ is a real number. However, we can express the frequency-domain transfer function of a given problem in terms of a complex frequency.

The SEM exploits a special feature of scattering and radiation from three-dimensional objects: the simple (i.e., first-order) poles their transfer functions may possess in the complex-frequency plane. If we know the locations and amplitudes (or residues) of these poles, we can easily construct a transient response, which is simply a series of exponentially damped sinusoidal terms, one for each pole. Much early work in SEM used frequency-domain analytical techniques to find the poles.[27,28] More recent work shows that the poles are extractable from time-domain data.[29,30] Because SEM provides a simple relationship between the frequency domain and time domain, we regard it as a hybrid technique.

ASYMPTOTIC TECHNIQUES

Asymptotic techniques may involve either low- or high-frequency characteristics of the frequency-domain approach, or the corresponding late and early responses of the time-domain approach.[13] In either case, asymptotic techniques attempt to exploit what is analytically deducible about time or frequency behavior for the limits indicated. For example, we can show that the radiated far fields produced by a pulse-excited finite-sized object as a radiator or scatterer must vanish as approaches 0. Therefore, we know that the time integral of the far-field waveform must also vanish.

Low-frequency asymptotic results may also be based on the Rayleigh law of scattering, whereby the fields go to zero with decreasing frequency as ω^2. In the high-frequency limit, we might employ physical optics, geometrical optics, or the geometrical theory of diffraction to obtain the asymptotic behavior.

MEASUREMENT

Transient-response data are measured primarily through direct time-domain procedures. Developments in short-pulse technology enable us to generate and measure high-amplitude ($>10^3$ v), fast-rise-time ($\lesssim$300 picoseconds) pulses.[31,32] By using these pulses to excite a test object such as a scatterer or antenna, and using a sampling oscilloscope to measure induced currents and scattered fields, instantaneous-measurement bandwidths of 10:1 and more are possible. Such data can validate time-domain calculations directly; transformed to the frequency domain, they can meet a variety of needs.

Physical Aspects of Transient Analysis

Perhaps the single most useful aspect of transient analysis is the opportunity it provides for more clearly depicting and interpreting the physical behavior of electromagnetic fields. For example, a short pulse propagating on an open-ended wire clearly demonstrates the effects of radiation damping, dispersion, and reflection from an impedance discontinuity. Because such effects are harder to interpret as a function of frequency, they must usually be indirectly inferred in the frequency domain. Of course, by

transforming frequency-domain results, we can derive the transient behavior which illustrates such phenomena, but direct development in the time domain is generally more tractable, and the concepts are easier to visualize.

In this section we discuss fundamental physical aspects of transient radiation and scattering from a heuristic viewpoint. We first present typical results of time-domain computations, then examine in some detail the phenomena thus illustrated. Next we consider radiation fields as a manifestation of charge acceleration. The section concludes with a brief summary of the characteristics of radiation and scattering processes.

SOME NUMERICAL RESULTS

The calculations presented here precede a detailed account of their mathematical and numerical aspects in the next two sections. They are included now to provide a mental image of some physical aspects involved.

Figures 1 and 3 show current and charge distributions on a straight wire excited by a voltage source at its center as an antenna, and excited by a tangential electric field of a normally incident plane wave as a scatterer. In both cases, the time variation of the exciting source is Gaussian, i.e., $\exp[-g^2t^2]$, and space distributions of current and charge are shown for several instants of time. Figures 2 and 4 show the resulting far fields in the broadside direction.

In Fig. 1 the current for the antenna divides into two pulses, approximately Gaussian in form and with a small oscillatory undershoot, which propagate outward from the source, accompanied by oppositely signed charge pulses. The pulses (current and charge) decrease in amplitude and spread out as they propagate from the source. Nearing the end of the wire, the charge pulses increase in amplitude, while the current pulses decrease, falling to zero amplitude at the end. After the reflection, the amplitude of both pulses diminishes, and the current reverses sign because the charge flow reverses direction. Initially the radiated field closely resembles the Gaussian shape of the exciting pulse with which it coincides in retarded time (allowing for propagation time), but then exhibits a slight negative undershoot. A large negative pulse in the radiation field coincides with the end reflection of the current-charge pulse.

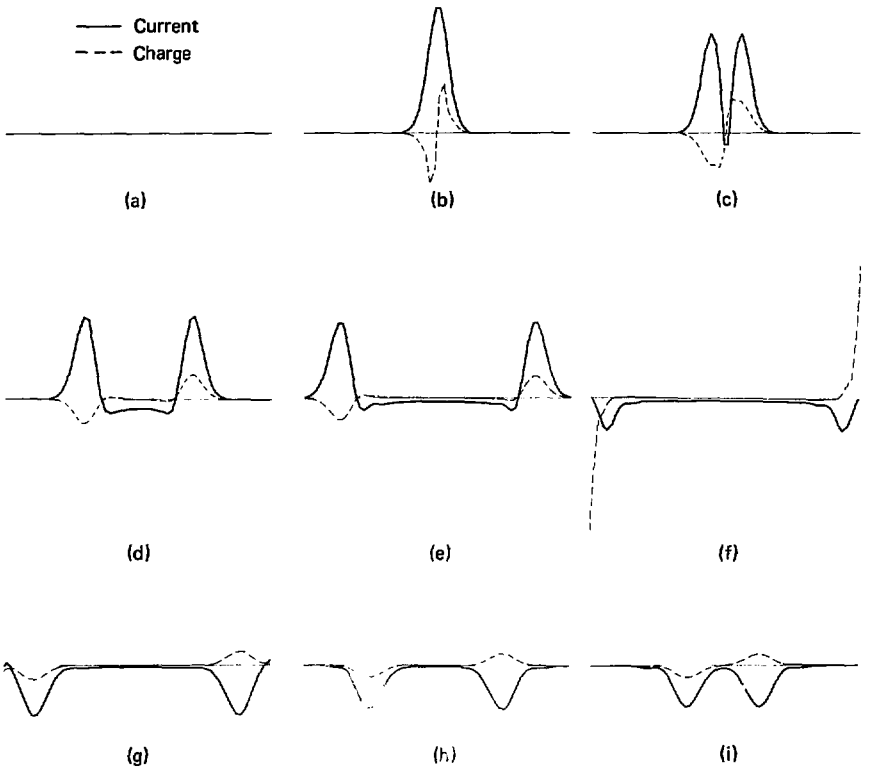

Fig. 1. Current and charge distributions at several instants of time for a straight-wire antenna excited by a Gaussian pulse. The antenna and numerical parameters are: length (L) = 1 m; radius (a) = 6.738×10^{-3} m (which gives $\Omega \equiv 2 \ell n L/a = 10$); Gaussian-pulse parameter g = 5.556×10^{-10} where the pulse time variation is $\exp[-g^2t^2]$; space-segment length (Δ) = L/60; and time interval (δ) = Δ/c. After its initial excitation, the charge-current pulse splits into two oppositely propagating pulses of oppositely signed charge, resulting in current pulses having the same sense. A slight decrease in the amplitude of the pulse can be observed as they progress down the wire, and a more noticeable decrease in amplitude occurs upon end reflection.

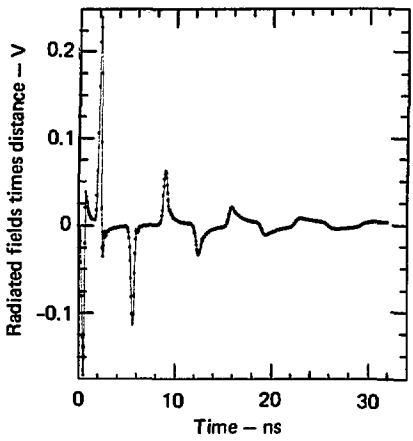

Fig. 2. Broadside-radiated electric field as a function of time for a straight-wire antenna excited by a Gaussian pulse. Six hundred time steps are shown. The peaks in the radiated field appear to coincide with the initial excitation and end reflection (in retarded time).

The current for the scatterer distinctly differs from that for the antenna. It is uniform over the entire wire except near the ends, where it falls to zero, and where the charge is first concentrated. We could deduce the current behavior in the scatterer from the current in the antenna by appropriately superimposing in time and space the result of simultaneously exciting the scatterer at a sequence of points along its length. The current amplitude in the central region of the wire slowly decreases with time, while near the ends it reverses sign as the boundaries of the pulse collapse inward due to the charge reflection. In the radiation (or scattered) fields, an initial return is similar in shape to the Gaussian exciting pulse and coincides in retarded time with the current buildup. This part of the scattered field is sometimes referred to as a specular flash. A sign reversal of the scattered field closely follows, with a peak value less than half that of the first maximum, beyond which the field decays with time. This part of the scattered field has a time variation similar to that of the decaying current.

INTERPRETATION OF NUMERICAL RESULTS

The relationship observed between the antenna current and radiation field clearly shows that the onset of current flow is responsible for the first portion of the radiated waveform. The subsequent negative pulse in the field is as clearly due to the reflection of the current and charge from the wire

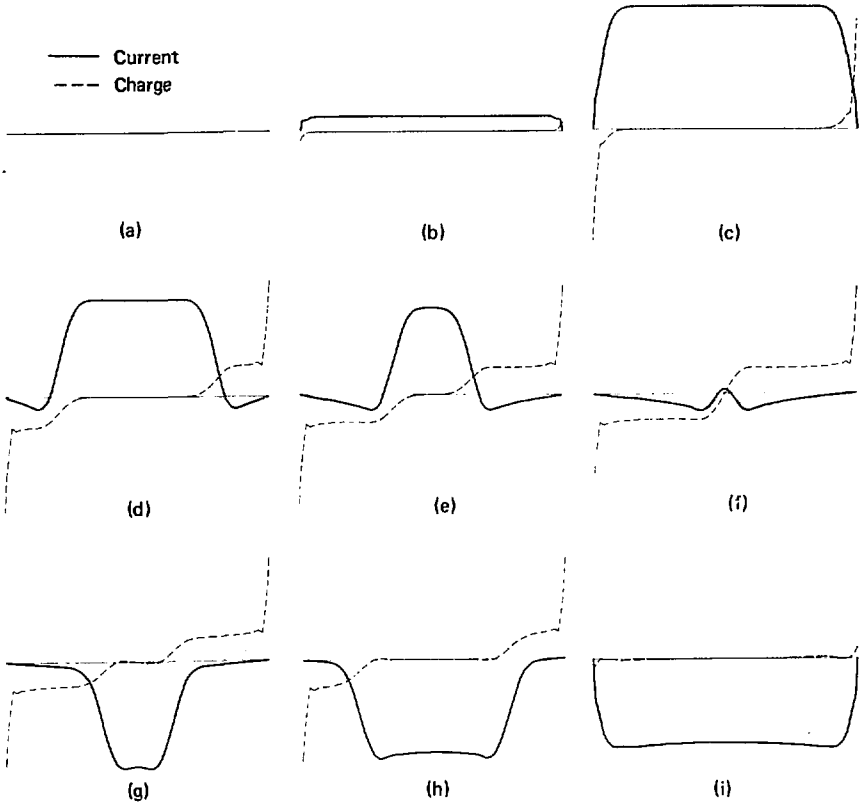

Fig. 3. Analog of Fig. 1 for the scattering case. The excitation is now a Gaussian-pulse plane wave incident from broadside. A uniform current is initially excited along the wire and collapses inward due to end reflection. No explanation has been developed for the small-amplitude oscillation in the current and charge of both Figs. 1 and 3.

ends. These results suggest that a radiated field is produced both when charge is accelerated (during turn-on of the current) and when charge is decelerated (during reflection from the wire ends). Note that the sense of the radiated field evidently depends upon the direction of the charge acceleration; the deceleration here corresponds to negative acceleration with respect to the original charge motion, and produces a field of opposite sign. The intermediate negative part of the radiated field is not so easily accounted

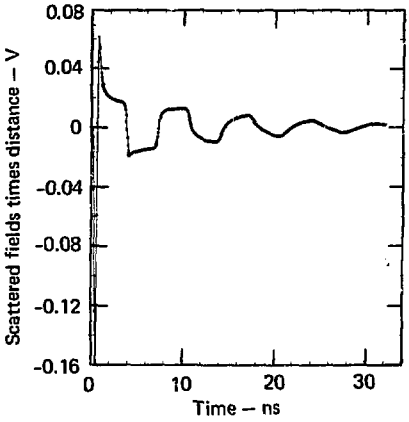

Fig. 4. Scattered field as a function of time for a straight-wire antenna excited by a Gaussian-pulse plane wave incident from broadside. The scattered field exhibits a specular-flash return as the current is first excited, then a longer lasting but slowly decaying portion of opposite sign.

for. It appears to correlate with the spreading out of the current pulse and with a corresponding decrease in its amplitude as it propagates down the wire. Thus, it could be ascribed to a shedding of energy during propagation.

The initial pulse in the scattered field is also clearly due to the initial charge acceleration associated with setting up the current. The nearly immediate sign change of the scattered field is evidently due to charge deceleration at the wire ends as the current begins to be reflected there. In this case the resulting negative radiation persists, although its value decreases with time, because current excited along the entire wire must eventually propagate to either end (recall that the antenna current divided into two oppositely propagating current pulses), where it is reflected. The decreasing amplitude of the scattered field in this portion of its waveform must be primarily due to the slow decay of the current reaching the ends, as demonstrated by the current behavior in the central area of the wire. This decrease in current amplitude provides further, although indirect, evidence that the current radiates as it propagates along the wire, and must therefore also contribute to the negative portion of the field at that time.

In both the antenna and scattering cases, then, we find evidence that accelerated charge causes radiation. This radiation occurs whether the charge is driven by an accelerating, exciting field which provides an external force, or by a decelerating, induced field which provides an internal or self force. The exciting force sets the charge in motion and produces the associated radiation fields. The induced force does no work on the charge but instead

receives energy from it as the charge slows to zero velocity. As the charge accelerates in the opposite direction, not all the energy returns to it. The difference is lost in the form of radiation. An additional loss seems related to a spreading charge pulse propagating on a wire, a result directly observable in the antenna case. The loss mechanism in this case might be the charge deceleration which the pulse dispersion implies. We might conclude that this behavior arises because the trailing edge of the pulse propagates more slowly than the leading edge, whose speed is near that of a light wave in the medium. Propagation of the charge pulse in this situation resembles the behavior of electron bunches in a klystron.

SOME MATHEMATICAL RELATIONSHIPS

It is indeed a fact that charge acceleration causes electromagnetic radiation. This fundamental principle provides a basis for a heuristic understanding of all radiation processes, both transient and steady state.

We can study accelerated charge fields in two ways: the microscopic approach, which concerns fields of individual charges, and the macroscopic approach, which concerns average fields over the charge distributions.[33] We primarily consider the latter approach here. We can distinguish between the two on the basis of whether the observation times and distances are smaller (microscopic) or larger (macroscopic) than the characteristic times and distances associated with the sources (e.g., the relaxation time in a metal or its skin depth). The microscopic approach involves equations of motion of individual electrons, and can include mass, relativistic, and quantum-mechanical effects. In the macroscopic approach, we are more interested in solving Maxwell's equations in a field description than in the physical details of their sources.

Using Maxwell's equations, the far-radiated fields due to an electric current distribution $\bar{K}$ over a surface S can be written

$$\bar{H}(\bar{r},t) = \frac{1}{4\pi rc} \int_S \frac{\partial}{\partial \tau} \bar{K}(\bar{r}',\tau) \times \frac{\bar{r}}{|\bar{r}|} \, ds' \tag{2a}$$

$$\bar{E}(\bar{r},t) = \eta_0 \bar{H}(\bar{r},t) \times \frac{\bar{r}}{|\bar{r}|} \quad , \tag{2b}$$

where $\bar{r}$ and $\bar{r}'$ are observation and source-point coordinate vectors,

respectively, t is the observation time, τ (the retarded time) is $t - |\bar{r} - \bar{r}'|/c$, and c is the speed of light.

Since $\bar{K}$ is by definition the flow of charge, any change in $\bar{K}$ with time, assuming charge is conserved, can be due only to a change in velocity of the charge which carries the current. Equation (2a) therefore states that radiation is due to accelerated (or decelerated) charge in agreement with the preceding discussion.

The fields of a point of charge q moving with (non-relativistic) velocity $\bar{v}$ and acceleration $\dot{\bar{v}}$ are

$$\bar{H}(\bar{r},t) = \frac{q\mu_0}{4\pi}\left\{\frac{\bar{v}(\tau)\times\bar{R}}{R^3} + \frac{\bar{R}\times[\bar{R}\times(\bar{R}\times\dot{\bar{v}}(\tau))]}{cR^4}\right\} \tag{2c}$$

$$\bar{E}(\bar{r},t) = \frac{q}{4\pi\varepsilon_0}\left\{\frac{\bar{R}}{R^3} + \frac{\bar{R}\times\bar{R}\times\dot{\bar{v}}(\tau)}{R^3 c^2}\right\}, \tag{2d}$$

where $\bar{R} = \bar{r} - \bar{r}'(\tau)$ and $R = |\bar{R}|$,

When $\dot{\bar{v}}$ is zero, $\bar{H}$ and $\bar{E}$ have $1/R^2$ static components, an elementary result, and $\bar{E}_{rad}$ changes sign when $\dot{\bar{v}}$ reverses direction. The rate of energy radiation is also given by[34]

$$\frac{dW}{dt} = -\frac{q^2|\dot{\bar{v}}|^2}{6\pi\varepsilon_0 c^3} . \tag{2e}$$

the total amount of energy radiation during a given velocity change is proportional to the time integral of $|\dot{\bar{v}}|^2$, so the higher the acceleration, the greater the radiated energy.

Equations (2c - 2e) represent a microscopic view of the radiation process. In our time-domain solution, we can develop expressions which provide a macroscopic description of the radiation process in terms of the current and charge distributions on the object. For the particular case of a wire object having contour C, the total energy collected by the object from the incident field up to time t is given by

$$W_C = W(t)\Big|_{\text{Collected}} = \int_{-\infty}^{t}\int_C \bar{E}_{inc}(w',t')\cdot\bar{I}(w',t')dw'dt' . \tag{2f}$$

Similarly the total energy dissipated due to resistive loss can be expressed

up to time t as

$$W_D = W(t)\Big|_{\text{Dissipated}} = \int_{-\infty}^{t}\int_C I^2(w',t')R(w')dw'dt' \quad . \tag{2g}$$

Finally, the total energy stored in the fields near the wire due to its current and charge density is, at time t, proportional to

$$W_W = W(t)\Big|_{\text{Wire}} \propto \frac{1}{4\pi}\int_C [\mu_0 I^2(w',t) + Q^2(w',t)/\varepsilon_0]dw' = W_I + W_Q \ , \tag{2h}$$

where W_I and W_Q are the current and charge contributions, respectively (see Appendix).

The energy in the fields outside the wire can then be represented as

$$W_F = W_C - W_D \propto W_W \quad , \tag{2i}$$

which represents the energy in both the radiation and the near fields. The quantity W_W usefully indicates the time-changing stored energy and, by implication, when and where radiation occurs.

THE ROLE OF CURRENT AND CHARGE

In the antenna case, the excitation is a tangential electric field applied at the center of a small region (the gap) of length Δ on the antenna's surface. For simplicity, assume the field is a unit-amplitude pulse of time duration δ, where $\Delta = c\delta$, applied at time t = 0. Our model is thus discretized in space and time and is conceptually identical to the numerical solution developed below.

Because the assumed perfect conductivity requires the total tangential electric field to be zero, initial application of the excitation instantaneously induces a charge separation, which results in both charge acceleration and current initiation. The tangential electric field of this separated charge cancels the applied field, and the linear charge density changes sign across the gap region. Due to the finite propagation velocity of the induced fields resulting from this charge motion and separation, the fields have no effect

outside a region of radius Δ centered in the gap during the time δ the excited field is applied.

Upon removal of the exciting field after a time δ, the charge separation in the gap must vanish to make the total field there zero. Simultaneously, a current and charge disturbance in the gap during $0 \leq t < \delta$ affects a region Δ wide on either side of the gap during the time $\delta \leq t < 2\delta$. This effect takes the form of a scattered tangential electric field having the same directional sense as that of the original charge separation in the gap. Consequently, a compensating net charge density in each of these regions must cancel this scattered field. Because of the continuity equation, this density is supplied by the movement of the charge out of the gap to the adjacent regions. Charge neutrality is thus restored in the gap and current flow there is zero. A current flow of half the original gap current is set up in these two adjacent regions. This current has half the original value because it involves the movement of only half the original charge (only the plus or minus charge, not both as in the gap). The current has the same sense on either side of the gap because it involves the oppositely directed flow of oppositely signed charges.

After a series of repeated steps like that above, these pulses of current reach the ends of the wire. The charges stop because the conduction current must vanish there. In stopping, the charges are subject to an oppositely directed acceleration and so produce a scattered field in a sense opposite to that of the original scattered field. A reflected charge and current pulse are thus produced, and the process described above continues, but with some loss due to radiation. From Eq. (2e), the amount of radiated energy is proportional to $|\dot{\bar{v}}|^2$; the shorter the time interval over which a given amount of charge reflects, the more the radiation loss. Thus, the narrower the incident pulse, the more efficient the radiation production upon end reflection.

We can analyze the scattering problem in the same way. Two factors which influence field and current behavior and which help us to understand the overall problem include: 1) causality, which limits the space-time region over which interactions can occur, and 2) the current-continuity equation, which constrains current and charge behavior. Energy is supplied to the object only while the exciting field is present. All this energy may be regarded as being radiated, but only a portion actually produces a space wave.

The rest remains tied to the structure along which it propagates. At each point where energy flow is redirected by the object, reradiation occurs. As in the source region, part of the energy leaves in a space wave and part remains tied to the structure. Where energy-flow redirection does not occur, as along a straight wire, there exists no radiation without dispersion, but only a continued propagation of fields previously produced.

THE FIELD BEHAVIOR

A prefectly conducting object can have an electric field as its surface in only the normal direction. The total tangential field is zero by definition. Without a normal field, there is thus no field at all. Consequently, for radiation to occur, there must be: 1) a non-zero charge density to produce a normal electric field, or 2) an incident field that is cancelled by an oppositely directed induced field. The latter cause of radiation is charge acceleration, as discussed above. The former is similarly associated with charge deceleration. The radiated electric fields may be closed (i.e., form continuous loops) or be open as a result of terminating on the object. They can close only as a result of charge cancellation, caused, for example, by meeting oppositely signed charges moving in opposite directions on a wire. All finite-sized, perfectly conducting objects produce radiation fields with closed lines at distances greater than the maximum object dimension.

Near fields, i.e., those field components that do not carry energy away from the object, include electric fields that terminate on the object due to its net charge density and associated magnetic fields that result from charge motion. These near fields contain the energy bound to the object's surface, which thus acts as a guided-wave structure for near-field energy propagation. Charge deceleration converts near-field energy to radiating energy. It is useful to think of energy due to charge separation as potential energy, and that due to charge motion as kinetic energy (see Eq. 2h). Both the fields and charge share the stored energy. Further, the charge terminates the fields on the conducting surface through the boundary conditions that E_{tan} and H_{norm} are zero.

SUMMARY

The following processes are primarily responsible for electromagnetic radiation:

1. Charge acceleration due to the incident field.
2. Charge deceleration due to reflection from impedance discontinuities such as open edges and steps on surfaces and open ends and bends on wires.
3. Charge deceleration due to surface curvature.
4. Charge deceleration along straight-line surfaces due to dispersion.

The observations made above are only qualitative, but can be used as a basis for predicting various aspects of radiation and scattering.

We may summarize the above discussion by invoking the following model for transient radiation from a perfect conductor. It is based simply on the fact that, due to the vanishing of the *total tangential electric field* on the conductor's surface, the *net energy flow* (Poynting's vector) across it must be *always identically zero*. During the time the exciting field (source) is present, the outward flow of energy due to the induced current and charge are thus exactly balanced by the source-supplied energy. After the exciting field becomes zero, therefore, there can be nothing other than zero energy flow normal (W_N) to the conductor's surface. But since the conductor must continue to radiate until all the energy is gone, we suggest that W_N has two counter-flowing components. One is an inward-flowing component which contains energy collapsing back onto the conductor from the fields near it. The other is an outward-flowing component which contains energy that propagates away from the conductor and is then lost.

Both components must remain the same as they decay monotonically with time until eventual charge neutrality is restored. Although the total near-field energy is not easily derivable from the current and charge, these induced sources provide a convenient and useful indication of the stored energy, and thus also of the radiation process, as we have seen above.

Mathematical Aspects of Transient Analysis

In this section we consider mathematical aspects of direct and transform techniques for obtaining transient results. We continue with a discussion of hybrid techniques that possess characteristics of both frequency- and time-domain analysis, and conclude by briefly discussing the limitations of these various approaches.

DIRECT TECHNIQUES FOR OBTAINING TRANSIENT RESULTS

From Maxwell's equations for a perfectly conducting closed surface we can derive two time-dependent integral equations based upon the electric and magnetic field, respectively, as the fo.cir, functions:[2]

$$\hat{n}(\bar{r}) \times \bar{E}_{inc}(\bar{r},t) = \frac{\hat{n}}{4\pi\varepsilon_0} \times \int_S \left\{ -\frac{\bar{R}}{R^2}\sigma(\bar{r}',\tau) - \frac{\bar{R}}{cR^2}\frac{\partial}{\partial\tau}\sigma(\bar{r}',\tau) + \frac{1}{c^2}\frac{\partial}{\partial\tau}\bar{K}(\bar{r}',\tau) \right\} \frac{ds'}{R} \; ; \quad \bar{r}\varepsilon S \qquad (3)$$

$$\bar{K}(\bar{r},t) = 2\hat{n}(\bar{r}) \times \bar{H}_{inc}(\bar{r},t) + \frac{\hat{n}}{2\pi} \times \int_S \left\{ \frac{1}{R}\bar{K}(\bar{r}',\tau) + \frac{1}{c}\frac{\partial}{\partial\tau}\bar{K}(\bar{r},\tau) \right\} \frac{\times\bar{R}}{R^2}\, ds' \; ; \quad \bar{r}\varepsilon S \; , \qquad (4)$$

where $\int_S$ denotes the integral $\lim \Delta S \to 0 \int_{S-\Delta S}$; $\bar{E}$ and $\bar{H}$, the electric and magnetic fields, respectively; superscript inc, the incident field; ε_0, the permittivity of free space; c, the free-space speed of light; $\bar{K}$ and σ, the surface current and charge densities; S, the surface of the object; $\hat{n}$, the outward-pointing surface normal; and

$$R = |\bar{R}| = |\bar{r} - \bar{r}'|$$

$$\tau = t - R/c \qquad \text{(retarded time)},$$

where $\bar{r}$ and $\bar{r}'$ are observation and source coordinates.

Equations (3) and (4) are the time-domain versions of what are often called the electric-field integral equation (EFIE) and the magnetic-field integral equation (MFIE), respectively, after the incident-field terms which appear in them. They are mathematically classified as Fredholm integral equations of the first and second kind, respectively, because the unknown appears only under the integral in the former, but outside it as well in the latter. Besides this important difference, which significantly affects their numerical treatment, they also differ in the order of the spatial singularities which occur when $R \to 0$. In the EFIE, the highest-order singularity is the $1/R^3$ of the $\sigma(\bar{r}',\tau)$ term, coming from the $\bar{R}/r^3$ factor, and the spatial derivative of $\bar{K}(\bar{r},\tau)$ which results from replacing $\sigma(\bar{r},\tau)$ via the continuity equation. The highest-order term in the MFIE, by contrast, is $1/R^2$. Finally, the MFIE is not as well suited to wires long compared with their diameter, because $\hat{n}$, being nearly parallel to $\bar{K} \times \bar{R}$, can produce numerical ill-conditioning. The far fields corresponding to Eqs. (3) and (4) have been given in Eq. (1).

Most frequency-domain antenna analysis is based upon the thin-wire approximation, which involves replacing a two-dimensional surface integration with a one-dimensional line integration, and approximating the surface current as an axially directed filament. This same approximation is also useful in the time domain. When applied to Eq. (3), it leads to

$$\hat{w} \cdot \bar{E}_{inc}(\bar{r},t) = \frac{\mu_0}{4\pi}\int_C \left[\frac{\hat{w}\cdot\hat{w}'}{R}\,\frac{\partial}{\partial\tau}\,I(w',\tau) + \frac{c}{R^2}\,\hat{w}\cdot\bar{R}\,\frac{\partial}{\partial w'}\,I(w',\tau) - \frac{c^2}{R^3}\,\hat{w}\cdot\bar{R}q(w',\tau)\right] dw' \;;\; \bar{r}\in C + a, \qquad (5a)$$

where

$$q(w',\tau) = -\int_{-\infty}^{\tau} \frac{\partial}{\partial w'}\,I(w',t')dt' \,,$$

$\hat{w}$ and $\hat{w}'$ are tangent vectors to the wire at $\bar{r}$ and $\bar{r}'$, respectively, C is the wire contour, a is the wire radius, and $\bar{r} \in C + a$ denotes that the field is to be evaluated on the wire surface. Other time-domain integral equations specialized to wire geometries can also be developed. Equation (5a) provides the basis for most of the subsequent discussion in this paper. The far-field

expression which corresponds to Eq. (5a) can be written

$$\bar{E}(\bar{r},t) = -\frac{\mu_0}{4\pi R}\int_C \left[\hat{w}' \frac{\partial}{\partial\tau} I(w',\tau) + c\frac{\bar{R}}{R}\frac{\partial}{\partial w'} I(w',\tau)\right]dw' \quad . \tag{5b}$$

TRANSFORM TECHNIQUES FOR OBTAINING TRANSIENT RESULTS

The frequency-domain counterparts of the time-domain integral equation are given by[2]

$$\hat{n}(\bar{r}) \times \bar{E}_{inc}(\bar{r}) = \frac{1}{4\pi i\omega\varepsilon_0}\hat{n} \times \oint_S \left\{\nabla' \cdot \bar{K}(\bar{r}')\nabla'\phi - \omega^2\mu_0\varepsilon_0\bar{K}(\bar{r}')\phi\right\} ds' \tag{6}$$

$$\bar{K}(\bar{r}) = \frac{1}{2\pi}\hat{n} \times \oint_S \bar{K}(\bar{r}') \times \nabla'\phi ds' + 2\hat{n} \times \bar{H}_{inc}(\bar{r}) \quad , \tag{7}$$

where

$$\phi = \exp[-ikR]/R \text{ and } k = \omega\sqrt{\mu_0\varepsilon_0} \quad .$$

HYBRID TECHNIQUES FOR OBTAINING TRANSIENT RESULTS

Hybrid techniques, with characteristics of both frequency-domain and time-domain analysis, include the frequency-augmentation technique and the singularity-expansion method discussed below. Other possibilities might also be identified, such as various asymptotic techniques mentioned above.

Frequency-Augmentation Technique

Bennett et al.[35] developed a technique to combine low- and high-frequency scattering information for an object to obtain its impulse response. The basic idea of this frequency-augmentation technique is to represent the impulse response of the object in the frequency domain, $H(\omega)$, as

$$H(\omega) = F_A(\omega) + H_A(\omega) \quad .$$

The first term, the augmentation function, approaches $H(\omega)$ as ω approaches ∞, and thus represents the high-frequency information referred to above. The augmentation function might come from either time- or frequency-domain

analysis, and could be based upon geometrical optics, physical optics, or other considerations. The second term, the augmented-frequency response, thus vanishes as ω approaches ∞, and is derived from low-frequency information as follows.

Consider, for example, that, using either the time- or frequency-domain approach, the actual low-frequency response function of the object is known up to some maximum frequency ω_m and is denoted by $\tilde{H}(\omega)$. Then define

$$\tilde{H}_A(\omega) = \tilde{H}(\omega) - F_A(\omega)$$

and note that

$$\tilde{H}_A(\omega) = H_A(\omega) \text{ for } \omega \leq \omega_m .$$

But since $H_A(\omega)$ is known to approach zero with increasing frequency, we can introduce some reasonable asymptotic function to represent this behavior and match it to $\tilde{H}_A(\omega)$ in the region below ω_m to obtain an approximation for $H_A(\omega)$ for all ω. If the function so chosen is accurate enough, then we obtain a combined numerical-analytical representation for $H_A(\omega)$. Finally, a Fourier transform to the time domain yields the desired impulse response, h(t). The augmentation function contains the singular, high-frequency part of the response, and can be analytically transformed to the time domain, thus avoiding the problem of trying to numerically transform a singular function. Only $H(\omega)$ needs to be transformed using a numerical FFT.

Singularity-Expansion Method

We have already mentioned the basis of the singularity-expansion method (SEM). Here we very briefly discuss some of its more obvious aspects. SEM stems from the observation that the late-time EM response (i.e., when the exciting field no longer is present) of an object has the form

$$f(t) = \sum_{\alpha=1}^{N} R_\alpha e^{s_\alpha t} .$$

This time function has a similarly simple complex-frequency representation,

$$F(s) = \sum_{\alpha=1}^{N} R_\alpha/(s - s_\alpha) .$$

Note that f(t) and F(s) may represent any measure of the object's response, including induced current, near field, and far field.

In time-domain solutions, then, the original problem is replaced by the new requirement to find the R_α and s_α. This requirement can lead in turn to two distinctly different approaches, depending on whether time-domain or frequency-domain data are available for this purpose. A procedure based upon Prony's technique has been successfully used to obtain poles from time-domain data.[29]

The s_α depend only on the object geometry. Thus, once determined, they characterize the object for any excitation. The R_α, on the other hand, depend on both the object geometry and its excitation.

LIMITATIONS

Our ability to obtain transient results is limited by the same factors that apply to the frequency domain. Analytical solutions are available for relatively few problems, and those that have been developed generally require extensive computations. Numerical techniques are limited primarily by what is computationally feasible. From a mathematical viewpoint, then, our ability to formulate transient problems greatly exceeds our ability to subsequently cast them in a numerically tractable format. However, alternate formulations may exist which could greatly reduce the numerical effort required for solving a given problem.

Generally, the numerical approach is most effective for frequencies up to and including the resonance region, for the relatively simpler geometries. Any increase in complexity of object geometry or environment can greatly reduce or even eliminate the possibility of using a numerical approach. This is one area where further formulational efforts might be directed.

Numerical Aspects of Transient Analysis

Both time-domain and frequency-domain integral equations may be reduced to forms suitable for numerical computation. We first consider a time-domain solution.

For clarity, we illustrate the direct, time-domain solution procedure for a simpler, or prototype, time-domain integral equation in place of the actual Eq. (5a). We thus consider

$$g(x,t) = \int_{-h}^{h} f(x',t')K(x,x')dx' \quad ; \quad -h \leq x \leq h \ , \tag{8}$$

where

$$t'(x,x't) = t - |x - x'|/c \ ,$$

the equation to be solved, where g is specified and f is to be found. Proceeding on an intuitive basis, we might decide to approximate Eq. (8) with a discrete sequence of samples for f as a function of both x and t. If we further choose some reasonable variation between these discretely sampled points (i.e., select an interpolation function) and also specify how the right and left sides of this sampled equation are related, then we can reduce Eq. (8) to a linear system in which the samples for f are the unknowns.

For practical purposes this procedure constitutes the moment method. The interpolation function mentioned, in the moment-method context, is called a basis function, and the relationship between the two sides of the reduced equation depends on a weighting or testing function. Let us now use a space-time pulse approximation for f, i.e.,

$$f(x',t') = \sum_{i'=1}^{N} \sum_{j'=1}^{j} U_{i'j'}A_{i'j'} \ ,$$

where $U_{i'j'} = 1$ if $\begin{cases} x_{i'} - \Delta/2 \leq x' < x_{i'} + \Delta/2 \\ t_{j'} - \delta/2 \leq t' < t_{j'} + \delta/2 \end{cases}$

and is zero otherwise, and $x_{i'} = \Delta i'$, $t_{j'} = \delta j'$. Let us also point-match the integral equation at the space-time sample locations x_i, t_j. Then we

formally obtain

$$g_{ij} \equiv g(x_i,t_j) = \int_{-h}^{h} \sum_{i'=1}^{N} \sum_{j'=1}^{j} U_{i'j'}A_{i'j'}K(x_i,x')dx'$$

$$= \sum_{i'=1}^{N} \int_{(i'-1/2)\Delta}^{(i'+1/2)\Delta} \sum_{j'=1}^{j} U_{i'j'}A_{i'j}K(i\Delta, x')dx'$$

$$\text{where} \quad \begin{matrix} i = 1,\ldots,N \\ j = 1,\ldots,N_T \end{matrix} \quad . \tag{9}$$

But since $t' = t - |x - x'|/c$, and upon using $\Delta = c\delta$, Eq. (9) simplifies to

$$g_{ij} = \sum_{i'=1}^{N} A_{i',j-|i-i'|} \int_{(i'-1/2)\Delta}^{(i'+1/2)\Delta} K(i\Delta,x')dx' \quad , \tag{10}$$

which associates with each $A_{i'j'}$ a spatial integral (or interaction coefficient) over segment i' at retarded time $j - |i - i'|$.

It is helpful to rewrite Eq. (10). Let us first denote the interaction coefficients by

$$Z_{ii'} = \int_{(i'-1/2)\Delta}^{(i'+1/2)\Delta} K(i\Delta,x')dx' \quad ,$$

so that

$$g_{ij} = \sum_{i=1}^{N} Z_{ii'}A_{i',j'} = Z_{ii}A_{ij} + Z_{i,i-1}A_{i-1,j-1}$$

$$+ Z_{i,i-2}A_{i-2,j-2} + \cdots + Z_{i,1}A_{1,j-i+1}$$

$$+ Z_{i,i+1}A_{i+1,j-1} + Z_{i,i+2}A_{i+2,j-2}$$

$$+ \cdots + Z_{i,N}A_{N,j-N+i} \quad . \tag{11}$$

We observe that the first term involves a sample at the time step j, while all other samples are for j-1, j-2, ... and thus are from earlier times. Upon solving Eq. (11) for A_{ij}, we then find

$$A_{ij} = \frac{g_{ij} - \sum_{i'=1}^{N}{}^{i} Z_{i,i'} A_{i',j-|i-i'|}}{Z_{ii}} \quad ; \quad \begin{matrix} i = 1,\ldots,N \\ j = 1,\ldots,N_T \end{matrix} \quad , \qquad (12)$$

where the summation excludes the term i' = i.

Equation (12) should forcefully demonstrate that at time step j the integral Eq. (8) can be solved as an initial-value problem by time-stepping, for if all values of A_{ik} are known for $k \leq j - 1$, then A_{ij} is completely specified by them and the present value of the forcing function, g_{ij}. This equation shows the explicit effect of causality and the finite velocity at which EM fields propagate, as an increasing time delay between a source at i' and its influence being observed at i (through the time index $j - |i - i'|$). In principle this factor permits solving Eq. (8) without matrix inversion, as further emphasized by the $Z_{ii'}$ coefficient matrix in Eq. (12).

We have of course simplified this discussion of the numerical solution by choosing an apparently simple integral equation and using pulse-basis and delta-weight functions. The TWTD[39] code used to generate the results presented here uses a nine-term polynomial basis, up to and including quadratic space-time variation, and delta-function weights. But the integral equation used here represents that which would apply to a straight wire, and so is realistic. It makes retarded time depend very simply on source-observation distance, i.e.,

$$t' = t - |x - x'|/c \quad .$$

Therefore, as we integrate the source space (x'), the space-time path described by x' and t' is a straight line, as illustrated in Fig. 5. This integration path furthermore passes diagonally through the center of each space-time sample "patch" (or A_{ij}), because the observation points are also located at the patch centers and $\Delta = c\delta$ was used everywhere. This path means that a single A_{ij} is associated with each $Z_{ii'}$. In general, the integration path can pass through two A_{ij}'s for integration over one space segment, so that a given $Z_{ii'}$ decomposes into two parts, one multiplying each respective A_{ij} value.

For example, if the space observation points are not co-linear (i.e., on the same line defined by the current sample), then t' and x' are not linearly related and in general

$$t' = t - \sqrt{(x - x')^2 + (y - y')^2 + (z - z')^2}\,/c$$

$$= t - \sqrt{\rho^2 + (s - s')^2}\,/c \quad ,$$

where s and ρ are cylindrical coordinates of the observation point relative to the line along which the source current flows. Figure 5 also shows other representative space-time integration paths.

The g term in Eq. (8) (or the g_{ij} terms in Eq. (12)) represents the actual excitation (or its sampled values) which excites the response f (or the sample values A_{ij}). Since we are dealing with an integral equation based on the electric field and specialized to a wire, g represents the tangential electric field distribution along the contour C of the wire. For a scattering calculation, and assuming a point-matching solution is employed (which is the

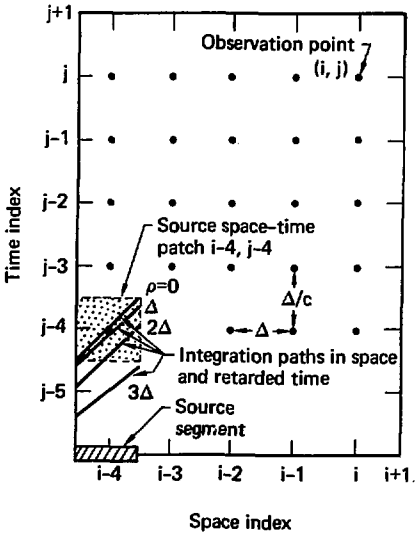

Fig. 5. Space-time integration paths in the source-coordinate (s',t') space for an observation point located at time t and cylindrical coordinates ρ and s relative to the center axis of the current filament (segment) being integrated. The retarded or source time t' is given by $t' = t - \sqrt{\rho^2 + (s - s')^2}/c$. Note: $s' = i'\Delta$; $s = i\Delta$; $t' = j'\delta$; $t = j\delta$. The uniformly spaced dots represent the centers of the space and time sample intervals for a straight wire, and the curves show the integration paths for a given source segment on that wire as ρ is changed. Note that unless $\rho = 0$ and s coincides with a space sample point (i.e., the observation point is collocated with the sample point on the wire), the integration over a single space segment can involve more than one time sample of the current on that segment. This shows one reason for using basis functions that smoothly vary over the entire space-time domain.

case for all the results subsequently presented), g_{ij} then is simply the specified value of the incident electric field tangent to C at a sequence of space points $\bar{r}_i$ and time steps t_j. For an antenna calculation, the exciting field is limited to one or a few segments of length Δ_i centered at observation point $\bar{r}_i$ and is equivalent to an applied voltage $V_{ij} = -\Delta_i g_{ij}$. The computation difference between a scattering and radiation calculation is minor.

The effect of lumped or distributed loads is mathematically indistinguishable from the treatment of the exciting source. The load causes a voltage drop in opposition to (passive) or in the direction of (active) the exciting field. The actual load voltage depends on its V-I characteristics. For linear, passive loads we have (resistance R, inductance L, capacitance C)

$$V_{LOAD}(\bar{r},t) = I(\bar{r},t)R(\bar{r}) + L(\bar{r})\frac{\partial}{\partial t} I(\bar{r},t) + C(\bar{r})\int_{-\infty}^{t} q(\bar{r},\tau)d\tau \quad ,$$

the effects of which can be readily included in the numerical treatment previously outlined. For example, this would result, in the case of our prototype integral equation, in

$$g(x,t) \rightarrow g(x,t) - V_{LOAD}(x,t) \quad ,$$

and considering a resistive load only at x_L, Eq. (12) becomes

$$A_{Lj} = \frac{g_{Lj} - \sum_{i'=1}^{N} {}^{L} Z_{i,i'} A_{i',j - |i-i'|}}{Z_{LL} + R_L} \quad , \qquad (12)'$$

while all other A_{ij}'s remain as given by (12).

When the load is non-linear, if for example the value of R_L depends on I_L, then formally Eq. (12)' still applies. But since R_L then depends on A_{Lj}, which in turn depends on R_L, we generally must solve the equation by iteration at each time step. For the special case of an ideal diode, however, which is specified by only a forward and reverse resistance, we can readily solve Eq. (12)' by finding A_{Lj} for $R_L = 0$, then using the direction of current thus determined to establish R_L, since the load cannot in this case reverse the current flow. We might also consider time-varying loads and other more general non-linearities.[36]

TRANSFORM TECHNIQUES FOR OBTAINING TRANSIENT RESULTS

Extensive literature on the numerical treatment of frequency-domain integral equations already exists.[2,37,38] We therefore will not consider that topic any further here.

DIRECT AND TRANSFORM TECHNIQUES COMPARED

Table 1 summarizes the main features of the direct time-domain and transform frequency-domain integral equations used to obtain transient results. The main differences between the two approaches are that: 1) the frequency domain provides source-independent results at a single frequency, so many frequency samples must be computed and transformed to find a transient result; 2) the time domain provides source-dependent results over the equivalent of a band of frequencies to give a transient result directly, but it must be repeated for each source, e.g., in computing the monostatic radar cross section. The corresponding computer times associated with their application are approximately[1,5]

$$T_t \approx (A_t N^2 N_T + B_t N N_T N_A) N_I \tag{13a}$$

$$T_f \approx (A_f N^2 + B_f N^3 + C_f N N_I + D_f N N_I N_A) N_F \quad , \tag{13b}$$

where $A_t,\ldots,D_f$ are computer- and algorithm-dependent timing coefficients, and the subscripts t and f denote time- and frequency-domain quantities, respectively. The two terms in T_t are due to current computation and far-field evaluation, where N_T is the number of time steps, N_I is the number of incident fields, and N_A is the number of far-field evaluations. In T_f we similarly have terms in order of their appearance due to impedance matrix calculation, matrix factorization or inversion, current computation, and far-field evaluation, where N_F is the number of frequency steps.

Upon introducing numerical values for the timing coefficients (for a CDC-6600), and relating the various numbers of current and field evaluations to the object size in wavelengths at the highest frequency of a transient calculation,[1] we find the following computer-time approximations for wire (subscript w) and surface (subscript s) objects excited by a single source ($N_I = 1$):

Table 1.

Frequency domain		Time domain
$\frac{\partial}{\partial t} = i\omega$	Maxwell's equations	Time dependent
$L(\omega)f(\omega) = g(\omega)$	Plus BC, etc.	$L(\tau)\ f(\tau) = g(\tau)$ $\tau = t - R/c$
$\sum_{j=1}^{N} Z_{ij}f_j = g_i$; αN^2 $i = 1,\ldots,N$	Apply MoM to get Nth order system	$\sum_{j=1}^{N} \tilde{Z}_{ij}\tilde{f}_{jk} = \tilde{g}_{ik}$ $i = 1,\ldots,N$ $k = 1,\ldots,N_T$
$f_i = \sum_{j=1}^{N} Y_{ij}g_j$; αN^3	Matrix manipulation yields	$\tilde{f}_{ik} = \sum_{j=1}^{N} \tilde{Y}_{ij}\tilde{g}_{jk}$; $\alpha N^2 N_T$
Solution obtained for many sources but single frequency.	Observe	Solution obtained for single source but for many frequencies.
Do for $\ell = 1,\ldots,N_F$ frequencies to get $f_{i\ell}$		

$\tilde{f}$ and f are related by

$f_{i\ell} \overset{\text{F.T.}}{\Longleftrightarrow} \tilde{f}_{ik}$

$$T_{t,w} \sim 10^{-1}(L/\lambda_{min})^3 \text{ s}$$

$$T_{t,s} \sim 7(C/\lambda_{min})^5 \text{ s}$$

$$T_{f,w} \sim [1 + 0.015(L/\lambda_{min})](L/\lambda_{min})^3 \text{ s}$$

$$T_{f,s} \sim [2 + 0.83(C/\lambda_{min})^2](C/\lambda_{min})^5 \text{ s} \quad .$$

Here L is the total length of the wire object, C is the circumference of the smallest sphere which can contain the surface object, and λ_{min} is the minimum wavelength for which the calculation is valid. Only the dominant terms from Eq. (13) have been retained. These results, plotted in Fig. 6, demonstrate

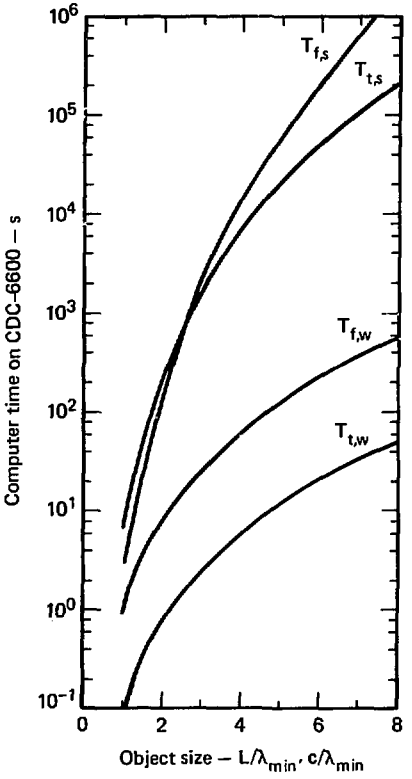

Fig. 6. Computer time estimates to obtain transient results for a single excitation for both wires and surfaces as a function of length and circumference in wavelengths at the highest frequency of the computation, and using both a direct time-domain solution and a transformed frequency-domain solution. A significant advantage for the wire time-domain approach over the frequency domain technique is shown. For surfaces, however, the difference is not as great, perhaps because the time-domain code used for this comparison[14] re-computes the interaction elements at every time step. This data should be regarded as approximate and only a guideline. Possible reductions due to symmetry were not included. Note that the surface-object time estimates are larger than given in Ref. 1 because more conservative sample-density estimates were used here.

the computational advantage of the time-domain approach to obtain transient results for a wire. For surface objects, on the other hand, the time-domain approach becomes more efficient only for C/λ_{min} values $\gtrsim 3$. These results indicate general trends only, since they are based on non-optimized codes and do not include the effects of symmetry or other influencing factors. They are useful, however, in drawing attention to an important aspect of transient calculations. Note that, for surface objects, computer time has a higher-order dependence on size because it involves an area, rather than a line, sampling of unknowns.

A further computer-related characteristic that differentiates a time-domain from a frequency-domain approach for transient computation is the computer storage required. Because a given surface current and charge sample are needed during the computation only for the time when their fields interact with the rest of the object, the storage required can be considerably less than the NN_T otherwise required.[1]

MODELING GUIDELINES

Because time-domain techniques involve more user decisions than their frequency-domain counterparts, in terms of temporal sampling and the time variation of the exciting field, they can be somewhat more demanding to use. If, however, the goal of the frequency-domain approach is to develop transient behavior via a transform, then similar decisions regarding frequency sampling and the spectrum of the exciting field are required. In each approach, these factors are important to both the efficiency and accuracy of the final result, but it remains unclear how to choose them *a priori* to most nearly attain the conflicting goals of computational speed and numerical accuracy. Also common to each is the need to spatially sample the object being modeled in a manner consistent with the temporal sampling and the accuracy-efficiency aspects of the calculation.

In our discussion of sampling questions above, the sampling density used the Shannon-Kotelnikov (also sometimes called Nyquist) rate of two samples per period of the highest frequency component in the waveform (or spectrum). But this value is an upper bound on the temporal-sampling interval and is attainable only when the basis function exactly matches the components in the waveform. In our example, the exponential time variation discussed in connection with SEM results in a damped, time-harmonic oscillation which

exactly represents the late-time free response of a conducting object so that the Nyquist rate does apply. Thus, the temporal- and frequency-sampling intervals have their maximum theoretically possible values when using the SEM representation. SEM also provides the most efficient representation and transform between the time and frequency domains for complex exponential functions via the LaPlace transform pair.

However, when the frequency and time domains are connected via the Fourier transform pair, the sampling intervals in time and frequency must be decreased because the basis functions (in this case, exponentials with purely imaginary arguments) are not the most appropriate for a waveform (or spectrum) of complex exponentials. One can better understand this fact by observing that a complex exponential can only be approximated, but not exactly matched, by sinusoids unless an infinite spectrum of such sinusoids is used. In practice, when using the FFT or alternate numerical transforms, we find typically that 10-12 samples per period of the highest frequency component are required to obtain acceptable accuracy.

The above discussion was included to emphasize that sampling densities are determined by several factors, and that theroretical expectations based on optimum conditions may not be met. More complete consideration of this question is given elsewhere.[16] Here we conclude our discussion by summarizing the following modeling guidelines concerning time-domain calculations for wires using the EFIF:

1) Space sample, Δ, should satisfy
$$2a < \Delta \lesssim \lambda_{min}/6 \quad ,$$
where a is the wire radius and λ_{min} the shortest wavelength of concern.

2) Time sample, δ, should satisfy
$$\delta \lesssim \lambda_{min}/6c \quad ,$$
where a lower limit is not given because the theoretical restriction that applies to the magnetic-field case where $\delta \gtrsim \Delta/c$ does not apply here.[9]

These sample intervals are smaller than the Nyquist rate, because the space-time basis function used (a nine-term 2nd-order polynomial) is only an approximation of the actual current and charge variations being modeled.

DEGREE OF APPLICABILITY

Problem types for which a computer model may prove suitable depend on the user's judgment of computer costs involved, the degree to which the model resembles the problem of interest, etc. The prospective user should be aware of various computation factors affecting potential applications. We categorize them as configurational factors (relating to the object), environmental factors (relating to the object's surroundings), and miscellaneous factors.

Configurational Factors

As a general rule, wire objects are more amenable to computer modeling than are surface objects, because they involve a linear rather than an area sampling. Wire objects successfully modeled in the time domain include straight and curved (modeled as piece-wise linear) wires, open- and closed-ended wires, wires having bends and multiple junctions, and wire grids. Surface objects modeled include smooth closed surfaces, closed surfaces with edges and vertices, and open surfaces (shells). Hybrid objects (i.e., objects having wire and surface features) have also been modeled.

Environmental Factors

The characteristics of the medium in which an object is located can have a very great impact on the feasibility of developing a computer model. Most results obtained to date apply to infinite, uniform, lossless, non-dispersive, linear, and isotropic media. A relatively simple extension is possible to handle up to three orthogonal, perfectly conducting image planes. Some work has also been done for a general, non-linear medium.[32]

Miscellaneous Factors

Other time-domain features available include the ability to handle lumped and distributed resistance, inductance and capacitance, and non-linear loads.

LIMITATIONS

The numerical implementation of direct time-domain techniques can be generally inferred from the list of applications mentioned above. But listing

a given problem does not necessarily mean that it can be modeled without difficulty. Many problems described are one of a kind and include features for which the treatment remains uncertain (e.g., sharp bends on wires, edges and vertices on surfaces). Furthermore, the solutions which have been worked out may be for special cases and not yet generalized (e.g., expansion for an axi-symmetric surface object for axial, but not oblique, incidence).

Perhaps the most serious limitation concerning direct time-domain computations, however, is the computing capability required. Even the CDC 7600* computer can be challenged by apparently simple wire calculations. For example, with a core of ~5×10^5 words available for variable storage, the time response of a straight wire having more than 150 space samples cannot be carried out in core for the minimum of four transit times required to obtain its poles (assuming $\Delta = c\delta$). Looked at another way, $2NN_T + 10N^2 \lesssim 5 \times 10^5$,† so that with $N_T \sim 4L/c\delta = 4L/\Delta$ and $N = L/\Delta$, we have $\Delta \gtrsim 6 \times 10^{-3}$ L. If samples are saved for only the time span L/c for which they are needed, then Δ can be reduced by only a small factor of less than 2, allowing a slight increase in the equivalent frequency range. If only the peak response or the energy collected is sought, then the computation might be completed much earlier than L/c. Generally, however, wide-band calculations can require substantial storage (and time) resources.

Experimental Aspects of Direct Techniques

A presentation of transient electromagnetics would be incomplete without mentioning the role of experimental measurements. Of course, as is true for analysis and computations, we can derive transient results from either direct or transformed measured data. Our concern here is with the former since frequency-domain experimentation is well known. In the discussion that follows, we outline a general approach to time-domain measurements, describe one particular facility, present some representative results, and summarize various applications for which such techniques might be considered. This approach was pioneered at Sperry Research Center.[31]

*Reference to a company or product name does not imply approval or recommendation of the product by the University of California or the U.S. Energy Research & Development Administration to the exclusion of others that may be suitable.

†The $2NN_T$ arises from storing current and charge information, and the $10N^2$ is due to other storage requirements.

TIME-DOMAIN MEASUREMENTS

The most significant difference between time-domain and frequency-domain measurements is that the former uses time-range gating to eliminate the need for the reflection-free environment the latter requires. A time-domain measurement is conceptually quite simple, requiring as a minimum an impulsive electrical source, a sensor, wide-band sampling oscilloscope to measure the sensor output, and associated cabling. Source characteristics primarily determine the overall bandwidth and signal-to-noise ratio of the transient experiment. Commercially available pulsers having rise times approximately 250-300 ps and peak voltages approximately 1-2 kV give useful maximum frequencies extending to 3-4 GHz. Pulsers with even faster rise times, approximately 100 ps, are available, but they have lower outputs and consequently lower signal-to-noise ratios.

The sensor used for time-domain measurements can be simple or elaborate, depending on the application. For determining the transfer or self-admittance of a wire antenna, for example, the antenna itself serves as the sensor. For determining surface current or charge density, we can use various probes based on loops or monopoles. If these probes are small relative to the object tested, their outputs will approximate the time derivative of the local magnetic or electric field. Therefore, they are often called B-dot and E-dot sensors, respectively. The AFWL recently developed a line of precision-designed and constructed sensors in lead arrangements for various applications.

Available sampling oscilloscopes can measure to 12-14 GHz and thus cover the bandwidths provided by current and anticipated pulsers.

Although only the items described above are essential for time-domain measurement, other components can crucially improve the accuracy and/or efficiency of a system. Perhaps most important is a mini-computer for data acquisition and processing. It can monitor and control the experiment and perform initial data processing such as smoothing, averaging, or FFT-transforming to the frequency domain. Coupled with peripheral equipment such as a magnetic tape unit or paper tape reader/puncher, it permits data storage for post processing. The data acquisition system can be supplemented by an X-Y plotter for real-time data presentation in hard copy.

Figure 7 is a block diagram of the LLL transient system,[32] including all the electronics and a schematic depiction of the ground-plane range, transmitting antenna, and test target in a typical measurement configuration.

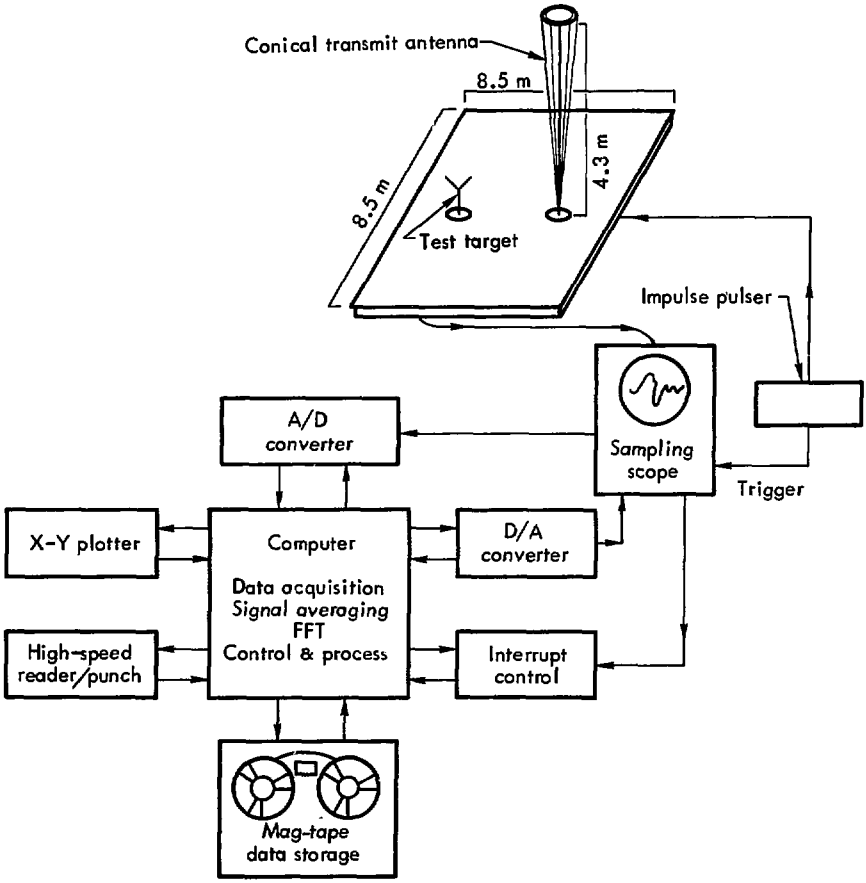

Fig. 7. Block diagram of a transient, ground-plane range shows its conceptual simplicity.[32] Major elements are the ground plane, pulser, signal-sampling oscilloscope, and computer data-acquisition, processing, and control components.

An advantage of the ground-plane arrangement is that the instrumentation cables can be introduced from under the ground plane, and are thus kept from interfering with the measurement. A disadvantage is that only objects having a symmetry plane can be measured, and polarization and incidence angles are limited. Time-domain measurements can be made in a free-space configuration as well, but, because isolating the cables is difficult, fiber optics or other nonmetallic data links may be necessary. Otherwise, only the early-time portion of the measured waveform may be uncontaminated by cable-induced artifacts.

The range clear time, which determines the low-frequency cutoff of the measurement, is established by the first arrival at the measurement point of a reflection from the walls or ceiling. In the LLL range, the clear time is 20-25 ns. Several other factors affect the overall quality of a given measurement, including the degree of wave-front planarity achievable over the target, the target-size-to-wavelength ratio at the highest effective frequency, the signal-to-noise ratio established by the pulser output and instrumentation, pulser time and amplitude stability, sensor sensitivity, and target-response characteristics. These factors are discussed more completely elsewhere.[32]

SOME REPRESENTATIVE RESULTS

Results obtained from two kinds of measurements performed on the LLL range are compared in Figs. 8 and 9 with calculations based on a thin-wire time-domain computer code. Figure 8 shows the input resistance and reactance of a base-fed monopole as functions of frequency obtained via an FFT from time-domain data. The experiment was performed by measuring the pulse reflected from a cable terminated at the ground plane with and without the monopole plugged into it, and computing the frequency-domain reflection coefficient from which the impedance is obtained.

The data in Fig. 9 are the transient response of a V-loaded monopole, presented as the voltage across a 50-ohm load. The computation includes the transmitting antenna (in this case a long (~4 m) straight wire), and the numerical exciting voltage is obtained from measuring the input voltage to the range antenna. Apart from a slight difference in the time base between the computed and measured result, they are in excellent agreement.

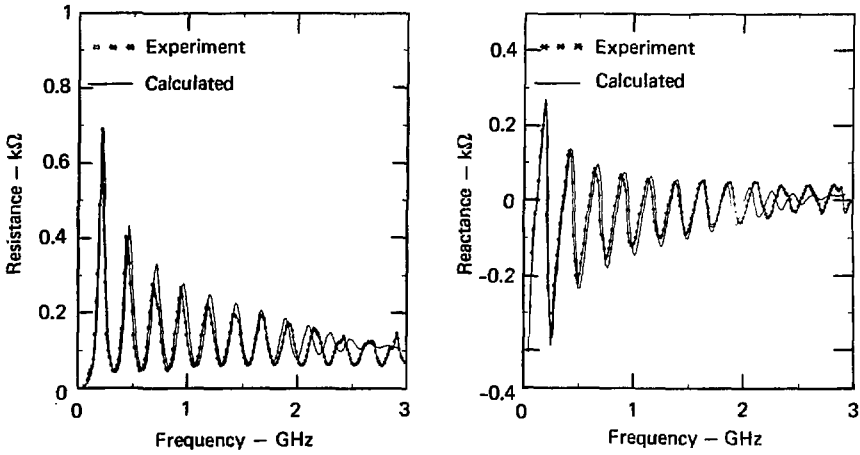

Fig. 8. Monopole impedance as a function of frequency as obtained from a time-domain calculation (——) and from transient-range measurement (****) transformed to the frequency domain using a FFT.[32]

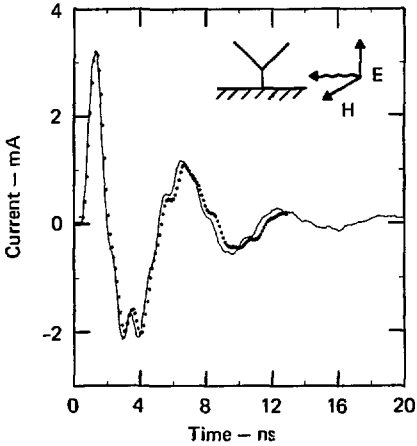

Fig. 9. Current induced on a V-loaded dipole as computed (****) using a time-domain approach and as measured (——) on the transient range.[32] The calculation model included the transmit antenna (a long monopole) and the measured voltage used to excite it. No normalization of the two results was performed; their absolute values are shown.

APPLICATIONS

Two kinds of direct time-domain measurements are illustrated above. The range of potential or actual measurement types is quite broad, and can be divided into two main categories, closed and open systems.

Closed Systems

Following the lines of time-domain reflectometry, we can measure constitutive parameters, system response functions, etc.[31] In closed geometries, such as coaxial lines and waveguides, geometric attenuation of the exciting field is not the problem it can be in open systems. Therefore, we can attain wider measurement bandwidths in the closed system with a given pulser.

Open Systems

The range of applications available in an open system includes transfer function, scattering, and input-impedance measurements. Input-impedance measurements are probably least demanding of these, because the input and output signals are not geometrically attenuated. The transfer-function measurement can be used for obtaining the transmitting and receiving patterns of antennas, while scattering measurements can be monostatic or bistatic. Measurements where the exciting field is incident on the sensor may reduce the dynamic range of the scattered field, because the sampling oscilloscope must be set on a range determined by the maximum input signal. Thus, for example, in measuring aperture-transfer functions, Babinet's principle may be impractical for replacing holes in planes by conducting plates.

The applications of time-domain measurements are of course similar in many ways to their frequency-domain counterparts. They are useful to validate analytical results and computer codes in either the time domain or frequency domain. More important, they can be used to generate data not derivable from analysis and thus provide information not otherwise available.

Applications

To convey the power and utility of transient analysis and to illustrate the methods used for a wide variety of problems, we now discuss applications of transient radiation and scattering techniques.

First, we explore a simple example in detail to acquaint the reader with the techniques and data-presentation methods. Several examples then illustrate salient features of transient analysis. We conclude with several examples intended to show the broad areas of applicability and to demonstrate physical interpretability.

EXAMPLE

We have chosen the linear dipole to demonstrate the techniques of transient analysis, since it is well understood and its properties are likely to be familiar to most readers. The results shown here were generated with the thin-wire code WT-MBA/LLL1B.[39]

The Linear Dipole as an Antenna

The time history of a narrow current pulse launched at the center of a 1-m-long dipole was shown by the current distribution at several sequential instants of time in Fig. 1. The forcing function was a tangential electric field applied to two segments (of total length 2Δ) at the center of the dipole of the form $E_{tan} = -1/2\Delta \exp[-g^2(t - t_0)^2]$V/m. This corresponds to driving the antenna with a zero-impedance voltage source of

$$V = \exp[-g^2(t - t_0)^2] \text{ volts.} \tag{14a}$$

As expected, the initial current pulse is nearly a replica of the applied voltage. The influence of the ends of the dipole is not seen immediately because of the finite propagation velocity of electromagnetic waves. Consequently, the initial current response is that of an infinite wire. This interesting aspect of the response is explored in further detail later.

The response seen in Fig. 1 is similar to what one would observe on a parallel-wire transmission line open at one end (the ends of the dipole) and shorted at the other (the center, source region of the dipole). Closer examination, however, reveals interesting differences between the dipole response and the parallel-wire-transmission-line response due to radiation associated with wave dispersion and end reflection. The effects of radiation are more clearly demonstrated in the curves shown in Fig. 10, where we have plotted $W_I(t)$ and $W_Q(t)$, as defined by Eqs. (2g-2h). W_I and W_Q initially increase rapidly as the voltage pulse is turned on, but then decrease with time, an effect we have previously attributed to radiation damping. When the current-charge pulse reaches the antenna ends, W_Q sharply increases, while W_I similarly decreases because the current flow vanishes there. After the reflection process, end radiation reduces both W_Q and W_I.

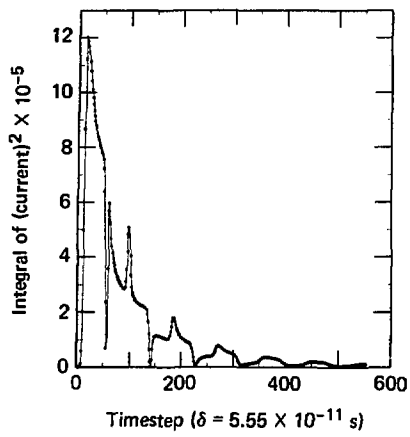

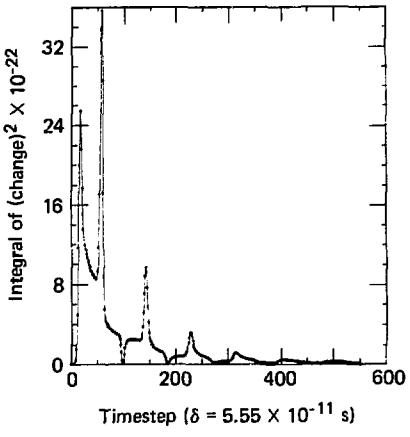

Fig. 10. Long-wire antenna results for the case already considered in Fig. 1. W_I and W_Q are derived from the integral over the antenna of I^2 and Q^2, respectively, and thus represent the energies stored on the wire in the current and charge. End reflection of the current-charge pulse (see Fig. 1) results in a substantial reduction of these quantities.

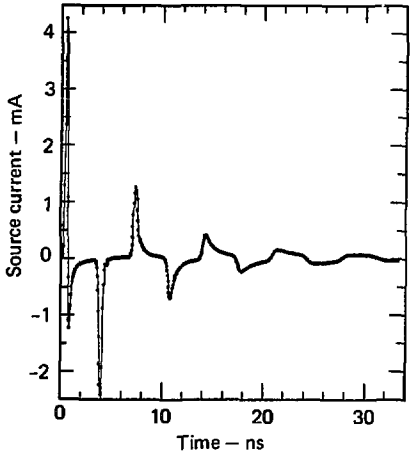

Fig. 11. Feedpoint current as a function of time.

This one simple calculation combined with proper presentation of data allows one to understand the dipole's characteristics in a natural and physically understandable way. This is not the only use we can make of the data, however. Consider the driving point (i.e., source region) current for this same antenna shown in Fig. 11, whose general form can be deduced from the

current of Fig. 1 at the dipole center. The driving-point admittance and impedance are

$$Y_A(\omega) = \frac{I(\omega)}{V(\omega)} = Z_A^{-1}(\omega) \ .$$

We can find either of these by taking the Fourier transform of the exciting voltage and the current of Fig. 11. The result for the impedance is shown in Fig. 12.

The driving-point characteristics agree with those found by other techniques, and specifically show that the input impedance is about 70 ohms at the first resonance, and that the first resonance occurs at a frequency slightly less than c/2L. The low frequency-input resistance found here also compares well with the classical value of[40]

$$R_r = 20\pi^2\left(\frac{L}{\lambda}\right)^2 \ .$$

The most fascinating aspect of transient electromagnetics is how these subtle aspects of the object's characteristics are folded into the transient

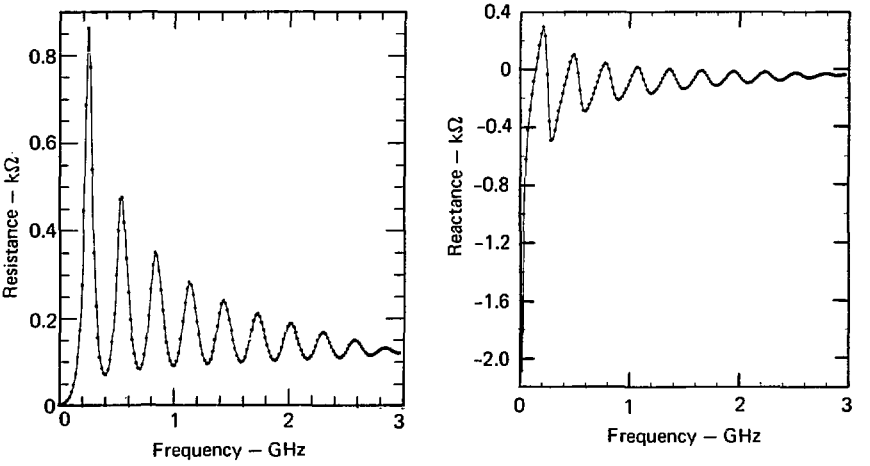

Fig. 12. Impedance-vs-frequency ratio obtained by using a FFT of the feedpoint current.

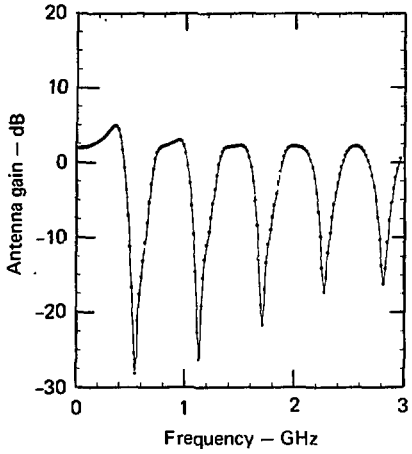

Fig. 13. Gain-frequency curve obtained by transforming the broadside-radiated field shown in Fig. 2.

response. We can explain the general behavior of the transient response quite naturally, yet the response contains features that one may not expect. Futhermore, the user finds the resonances naturally and does not have to seek tediously for them. The resonances occur where they will, and a single computation produces each one within the frequency range of valid results.

Figure 2 shows the broadside radiated far field of this dipole as a function of time. Figure 13 presents the broadside antenna gain in the frequency domain found from

$$G(\omega) = |\overline{E}_{rad}(\theta = \pi/2, \phi)|^2 / \int |\overline{E}_{rad}(\theta, \phi)|^2 d\theta \quad .$$

The known low-frequency broadside gain of 1.5 (1.76 dB) of a dipole is checked by our results.

Figure 14 illustrates the effects of loading the dipole at its center by various values of resistance. Here, the time variation of the driving-point current is shown for various values of resistive loading. A load having a value near that of the radiation resistance at resonance (~70 ohms) changes the current very little, while the 1000-ohm load appears to nearly critically damp the response.* This illustrates that the current pulses are propagating on the wire with a wave impedance near 1000 ohms. To minimize late-time

*The critical damping-resistance value depends approximately logarithmically upon the fatness parameter Ω.

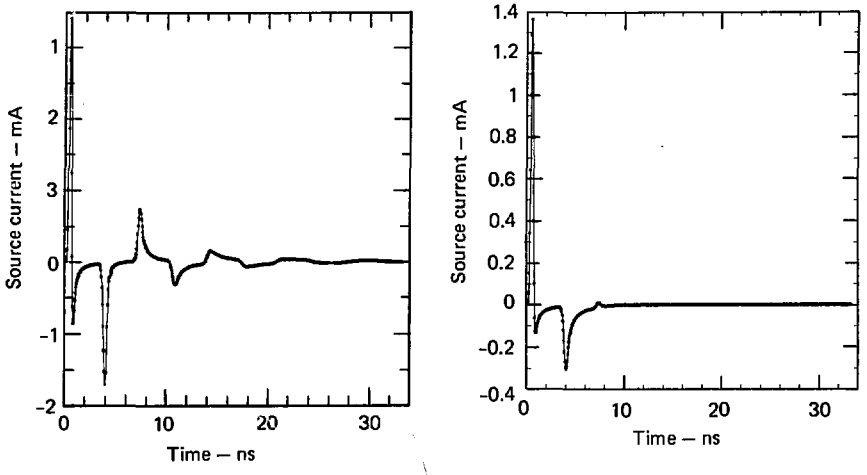

Fig. 14. Transient response of a long-wire antenna as affected by a resistive load at its feedpoint, shown by its feedpoint current. Nearly critical damping is observed for a resistance value of 500 ohms.

currents (in EMP protection, for example), one should thus choose loading that matches this wave impedance and *not* the radiation impedance of the structure at its dominant resonance. Such is the insight provided by direct time-domain analysis.

Figures 15 and 16 illustrate the effects of inductively loading the dipole. At a frequency half that of the lowest resonance, $f \cong 75$ MHz and $Z_{in} \cong -j450$ ohms. If the dipole is loaded at its feed point with an inductance of value $L \cong 0.95$ μH, so that $\omega L = +j450$ at 75 MHz, the dipole is then made resonant at ~75 MHz. Figure 15 shows that the dipole rings at this lower frequency if the indicated value of inductance is placed in series at the feed point. In Fig. 16 the input resistance is unchanged from Fig. 12, and the input reactance is modified by the additive term $2\pi fL$.

The Linear Dipole as a Scatterer

The short-pulse response of the dipole as a scatterer was previously shown in Figs. 3 and 4. In that case the excitation was a plane wave normally incident on the dipole with an electric field of the form

$$E_{inc} = \exp[-g^2(t - t_0/c)^2] \text{ V/m} \quad . \tag{14b}$$

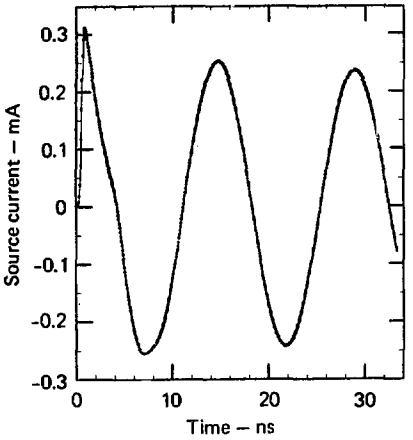

Fig. 15. The result of including an inductive load (L = 0.9524 μH) at the feedpoint is shown here by the transient feedpoint current, which, because it oscillates at about half the lowest resonance frequency of the antenna, radiates very slowly.

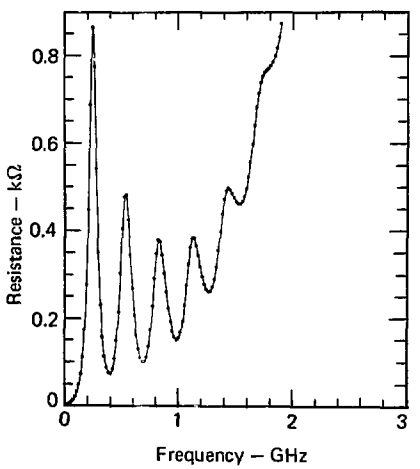

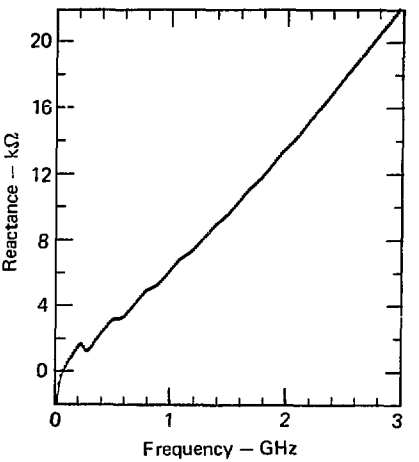

Fig. 16. Impedance in the frequency domain that results from including an inductive load at the feedpoint. The increase in the resistive component beyond $L/\lambda \sim 3$ is due to numerical inaccuracy and increasing dominance of the inductive reactance.

We discussed the antenna results with respect to the stored energy. Here, in Fig. 17, we present the corresponding results for the scattering calculation. The behavior of W_I and W_Q is quite different from the antenna case, and does not show radiation effects as clearly.

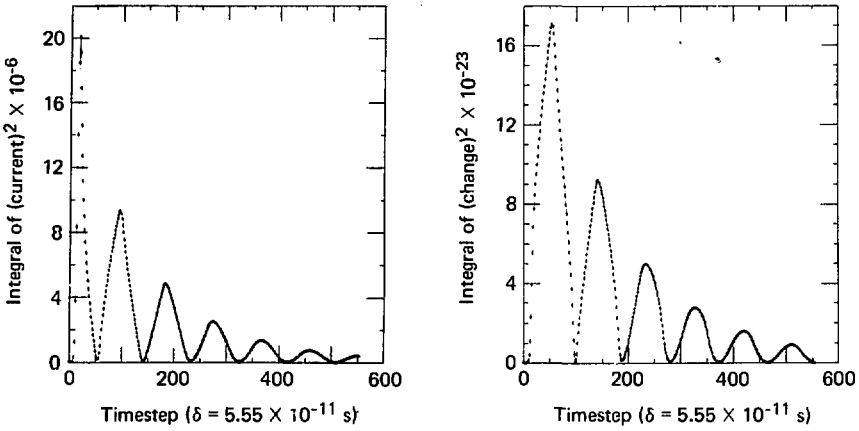

Fig. 17. Current and charge energy, W_I and W_Q, stored on a long-wire scatterer for the case already considered in Fig. 3.

In the scattering case, one can define a transfer admittance in the frequency domain which relates the short circuit current at the center of the wire to the incident field according to

$$Y_T(\omega) = \frac{I_{sc}(\omega)}{E_{inc}(\omega)} \quad ,$$

where $I_{sc}(\omega)$ is obtained from the transient response of Fig. 18. The effective height of the antenna is then given by

$$h_e(\omega) = Y_T(\omega) Z_A(\omega) \quad .$$

Figure 19 shows the transfer admittance of the dipole, and Fig. 20 shows the effective height. The effective height below resonance is ~0.5, increasing to 0.64 at the first resonance, which agrees with other results.

We can also find the frequency dependence of the scattered field. We use the time-domain back-scattered field for broadside illumination (Fig. 4) to obtain the familiar backscatter cross section shown in Fig. 21, where

$$\sigma(\omega)/\lambda^2 = \lim_{r \to \infty} 4\pi r^2 \left| \frac{\bar{E}_{scat}(\omega)}{\bar{E}_{inc}(\omega)} \right|^2 \quad .$$

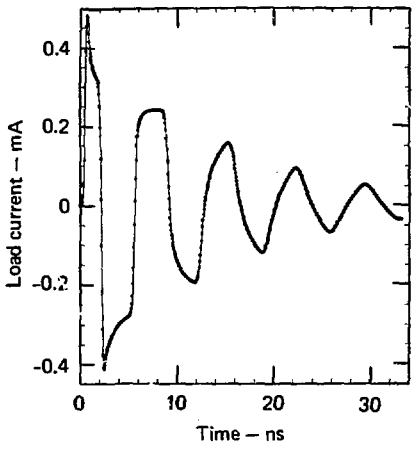

Fig. 18. Transient current at the center of the long-wire scatterer.

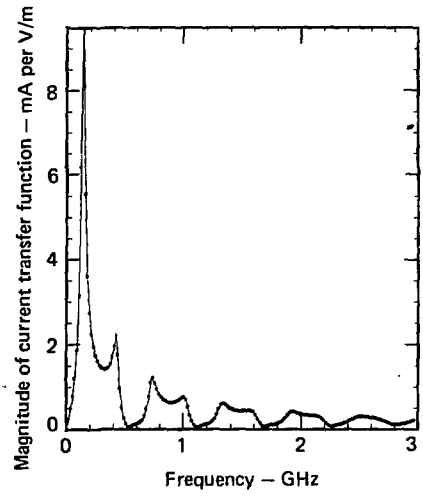

Fig. 19. Transfer admittance, obtained by transforming the transient current.

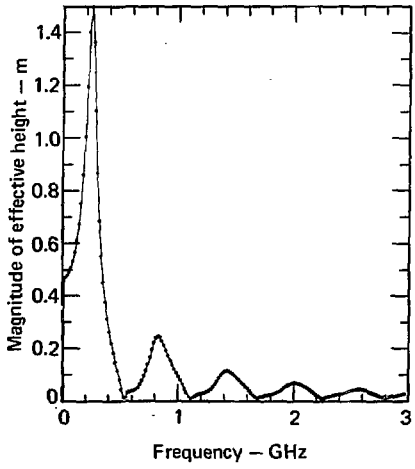

Fig. 20. By using the transfer admittance of Fig. 18 and the input impedance of Fig. 12, we can find the effective height, shown here.

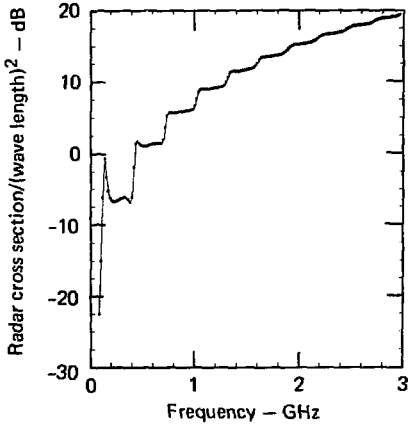

Fig. 21. Transforming the scattered field of Fig. 4 leads to the radar cross-section results shown here.

One could continue indefinitely along this line, studying the effects of loading, varying angles of incidence and observation, various pulse widths and shapes, various radii of wire, etc. We instead conclude here our direct time-domain analysis of the dipole and encourage the interested reader to pursue this further on his own.

SALIENT FEATURES UNIQUE TO DIRECT TIME-DOMAIN ANALYSIS

Inherently Broadband Calculations

The frequency-domain analysis of a structure is limited to discrete-frequency samples. The user of the code must choose *a priori* those frequencies where he thinks the structure will have interesting or useful behavior. If he chooses incorrectly, he may need to continue the calculations until he obtains the needed information, and can thus be reasonably confident that essential aspects of the object's behavior have not been overlooked.

The time-domain analysis of a structure, on the other hand, is inherently broadband. As long as the excitation contains sufficient energy in the frequency range of interest, the entire response over that range is automatically obtained. For example, consider a frequency-independent antenna, the conical spiral. However, this frequency independence occurs over some limited bandwidth where the antenna was designed to operate. If one needs characteristics over a wider band (for pulse applications or EMP coupling analysis), transient analysis conveniently provides them. In Figs. 22-26 we show some characteristics of a typical conical spiral. Figure 22 includes the feed-point current resulting from a Gaussian excitation (Eq. 14a) with a 350-ohm source impedance.[41] Transforming this current to the frequency domain yields the input impedance (corrected to remove the generator resistance) presented in Fig. 23. The calculation produces many low-frequency resonances of very high Q. The frequency-independent region of this particular conical spiral is fairly narrow, from 1.2 GHz to about 3 GHz. To help explain the origin of the low-frequency resonances, we plot input impedance on a Smith chart in Fig. 24. The spiral acts very much like an open-circuit transmission line at low frequencies, because it is basically a twisted pair of wires, with the wire separation increasing slowly. Consequently, the observed resonances are expected and qualitatively explainable from transmission-line theory.

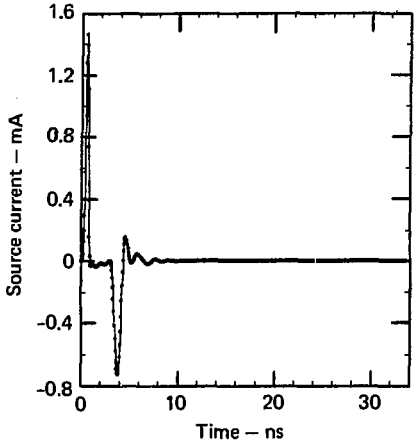

Fig. 22. Feedpoint current for a conical-spiral antenna excited by a Gaussian pulse. The effect of a 350-ohm series resistor is included. The numerical model consists of a piece-wise linear approximation (60 segments) to the actual antenna, whose total length is 1 m and radius is 1 mm, and which has two arms of 2 1/2 turns wound on a cone of half-angle 10° with small-end and large-end diameters of 3.36 cm and 9.16 cm, respectively.

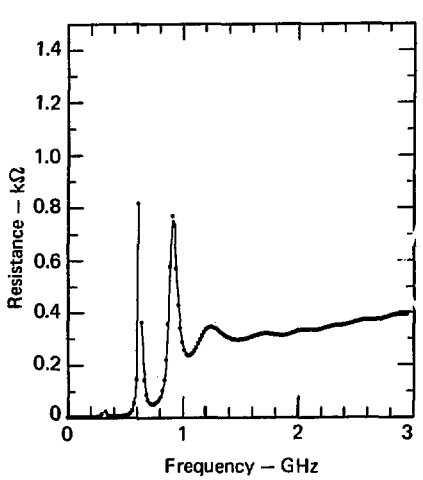

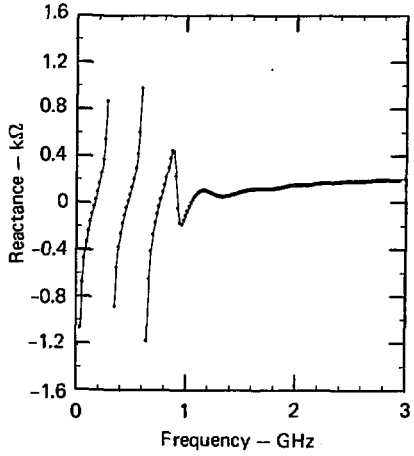

Fig. 23. Impedance for a conical-spiral antenna excited by a Gaussian pulse, obtained by transformation to the frequency domain. The late-time ringing of the spiral that would otherwise occur is damped out by the resistor and has been subtracted from the resistance curve.

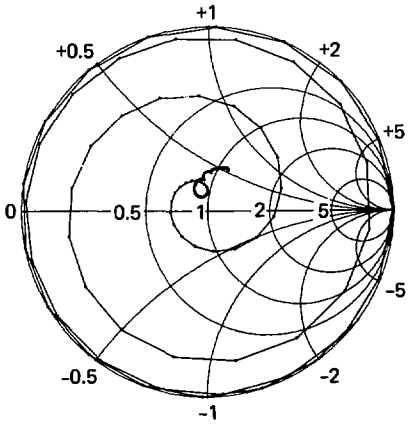

Fig. 24. A Smith-chart plot of the impedance emphasizes the spiral's similarity to an open-circuit transmission line below its frequency-independent operating band.

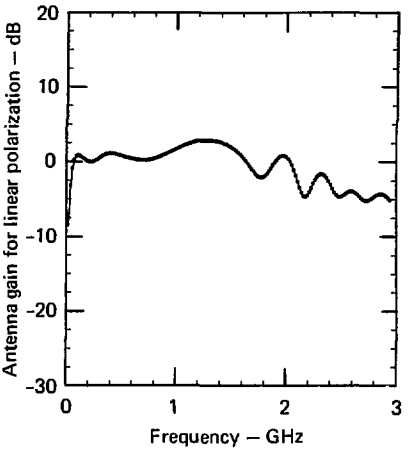

Fig. 25. The transmitting gain of the spiral.

To assess the importance of these resonances, Fig. 25 shows the bore-sight gain of the spiral for transmission, and Fig. 26 shows the magnitude of the short-circuit-current transfer function for reception (for linear polarization and the E-field parallel with the vertex wire). These calculations show that the spiral radiates or receives poorly at the low frequencies where the resonances occur. This result is expected, because high Q resonances involve little energy interchange per cycle.

Self-Diagnosis

One may encounter many pitfalls in applying any numerical technique. A peculiarity of direct time analysis that can be used to advantage is the way the results display ill-conditioning. For example, experience shows that the code WT-MBA/LLL1B requires that wire segments be at least as long as their diameter. In Figs. 27-29 we show the current on a dipole excited by a broadside-incident, Gaussian-pulse plane wave as a function of the wire radius, a. In each case, the dipole length is 1 m, the segment length (Δ) is 1.666 cm, and the Gaussian factor (g in Eq. (14a)) is 5.556×10^{-10} s^{-1}. The series of curves in Figs. 27-29 show the result of increasing the wire

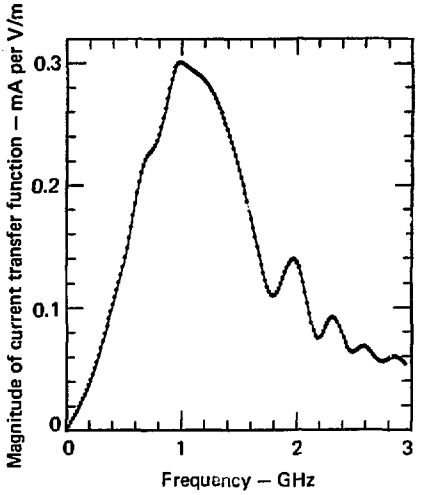

Fig. 26. The spiral's transfer admittance for reception.

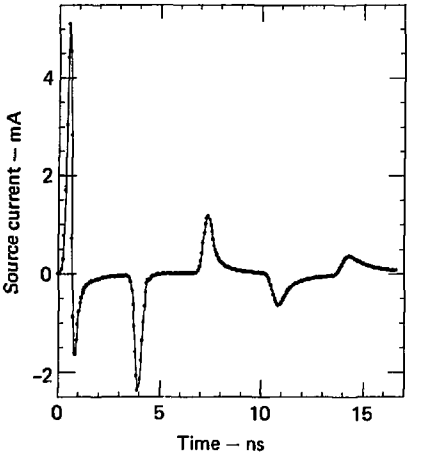

Fig. 27. Solution instability caused by use of too-short segments. The transient current on a 1-mm straight wire modeled using 600 segments (Δ - 1.66 cm) is displayed here for a wire 9 mm in radius.

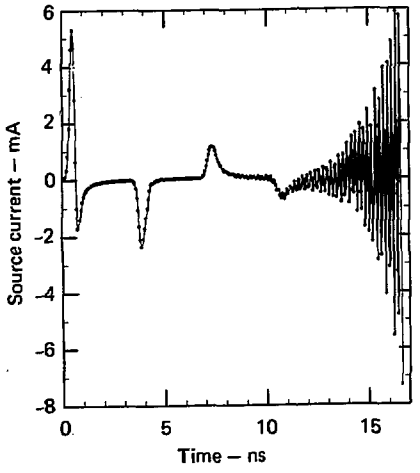

Fig. 28. Transient current for a wire 9.5 mm in radius. The divergent solution that occurs when $\Delta/2a > 1$ is evidently due to numerical inaccuracy of the thin-wire approximation.

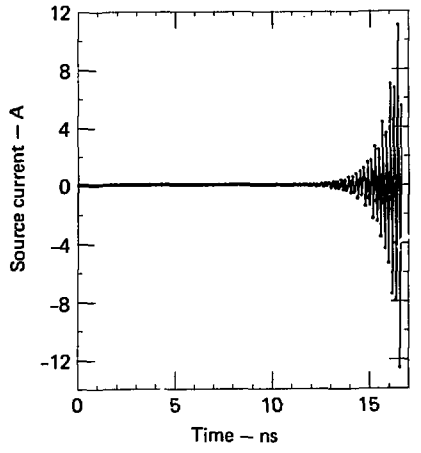

Fig. 29. Transient current for a wire 10 mm in radius.

radius, and consequently decreasing the ratio of segment length to diameter. As long as the segments are longer than a certain critical value, the current is well behaved and not a function of the number of segments. (Of course, if too few segments are used, the results will be inaccurate.) The exponentially growing current obtained for $\Delta \lesssim 2a$ signifies that something has become ill-conditioned. The particular source of this phenomenon in the numerical procedure has not been found, but is apparently a result of the thin-wire approximation. While the impedance matrix or interaction coefficients display nothing obviously wrong, the growing currents clearly signal that something in the numerical model is in error, however. Similar instabilities have been observed if only a single segment is too short, or if the match point of one segment lies inside the volume of another segment.

The user should realize, however, that merely obtaining responses that do not diverge in time does not guarantee that the calculations are valid. The final validation of results depends on a more thorough examination.

Direct, Efficient Responses

We have already pointed out that direct time-domain analysis is efficient for calculating the transient response of metallic objects. A single calculation yields the time history of the response for the entire object. This feature permits calculation of quantities that may be of interest in pulse applications, such as EMP-coupling studies, and that would otherwise be difficult to obtain, such as collected energy W_C and dissipated energy W_D. These quantities can be easily calculated using a direct time-domain approach and are directly useful in an EMP context.

For example, the coupling of EMP to a 10-m-long dipole resistively loaded at its center is presented in Figs. 30-32 as a function of the resistance value. The load current is shown in Fig. 30, the energy collected by the wire in Fig. 31, and the energy delivered to the load resistor in Fig. 32. Studies similar to these have been very useful in studying the transient behavior of other scatterers. From such studies, interesting results have emerged. For example, Figs. 31 and 32 illustrate that nearly all the short-circuit energy collected by the dipole can be delivered to a pure resistive load of about 1000 ohms. This result is unexpected from classical frequency-domain concepts, although a complete frequency-domain analysis gives the same result as found here, albeit with less physical insight. This finding also

corroborates the previous antenna calculations, where a 1000-ohm load was found to (approximately) critically damp the feed-point current.

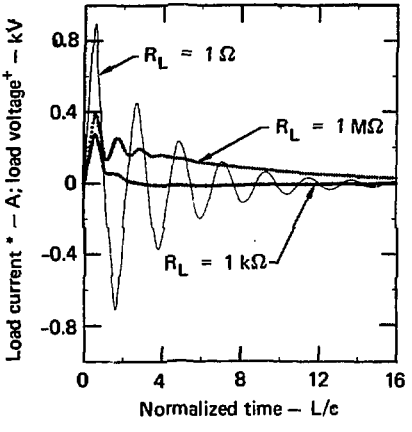

*Applies to R_L = 1 Ω and R_L = 1 kΩ only.
+Applies to R_L = 1 kΩ and R_L = 1 MΩ only.

Fig. 30. EMP applications of time-domain solutions. A 10-m-long wire of radius 6.738×10^{-2} m and modeled with 30 equal-length segments is illuminated from broadside by a nominal EMP pulse given by 5.25×10^4 [exp(-4 $\times 10^6$t) - exp(-4.76 $\times 10^8$t)]v/m. The midpoint current and voltage that result for several midpoint load values are shown here.

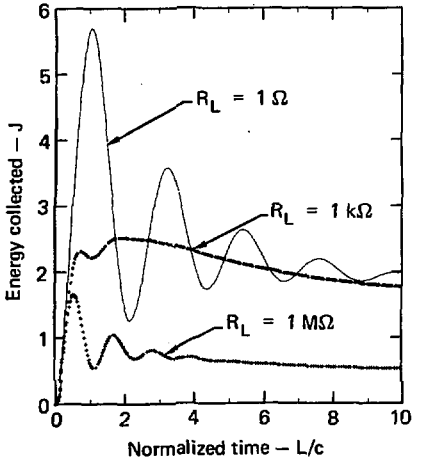

Fig. 31. Cumulative energy collected from the pulse by the wire, shown as a function of time (see Eq. 2). Observe that the collected energy is oscillatory in time, signifying the re-radiation of energy.

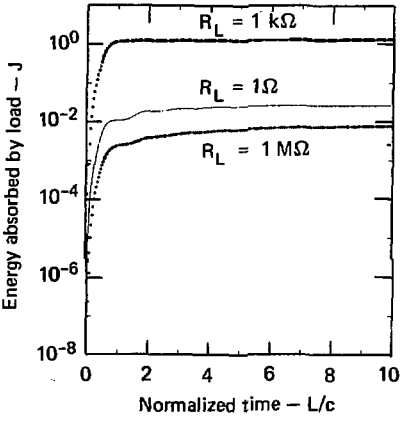

Fig. 32. Energy dissipated in the load as a function of time.

Nonlinear Capability

Solution formulation directly in the time domain permits analysis of nonlinear problems by a time-stepping procedure. This approach has been used with finite-difference techniques to handle the problem of a metallic object immersed in a nonlinear medium.[42] Schuman[43] and others[44,45] also consider a thin, straight wire loaded at its center by a diode. This case, as well as nonlinear loading of more general wire geometries, is possible using the approach developed by Miller, Poggio, and Burke.[17]

Here, we concentrate on the Miller, Poggio, and Burke approach. Figures 33-35 shows the response of a linear dipole antenna loaded with a diode. The diode was placed in series with a Gaussian voltage source. Figure 33 shows early-time history of the current and charge distribution along the structure. The dipole is initially biased in the forward-conducting direction, allowing a charge separation to build up across it. When the exciting voltage decreases to zero, the accumulated charge then reverse-biases the diode, allowing only a small leakage current in the reverse direction. The dipole then responds as two shorter dipoles placed end to end but insulated from each other. Comparison of the diode current and the unloaded dipole current (Fig. 11) illustrates that the initial current is essentially the same for these two cases (there is a slight amplitude difference caused by different wire radii) until the current in the linear case changes sign. From then on, the two currents are distinctly different. The late-time far field radiated broadside from the dipole is predominantly a dampened sinusoid at twice the frequency of the unloaded dipole, as shown in Fig. 35.

Combining an electromagnetic time-domain code with a time-domain circuit code such as SCEPTRE is feasible, but has not yet been implemented. Such a combination would be useful for studying the effects of loading an antenna with a complex nonlinear circuit. Some initial attempts at assessing these effects have been made with simple antenna models.[46] However, the proposed hybrid code would be able to analyze arbitrary antenna geometries.

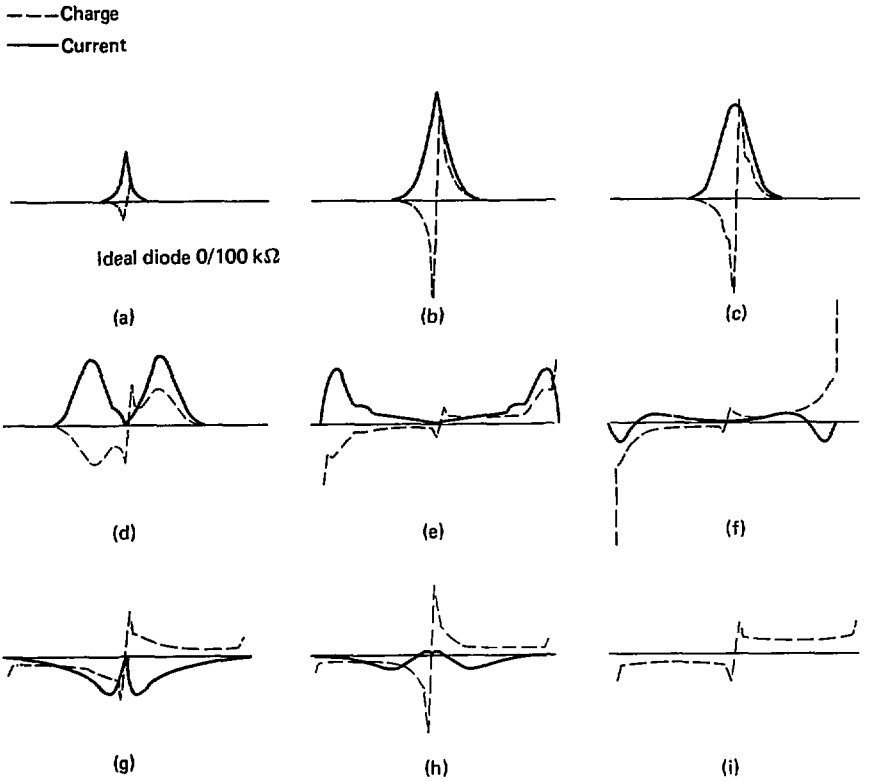

Fig. 33. Nonlinear loads can be easily handled in the time domain. Here the current (—) and charge (---) distributions on a 1-m center-fed dipole having a diode load in series with the generator are shown at several instants of time. Observe that the diode presents zero impedance only to current flowing in the initial direction, and that it effectively acts as an open circuit in the opposite direction (impedance = 100 kΩ). The two halves of the dipole thus retain a static charge distribution at late times.

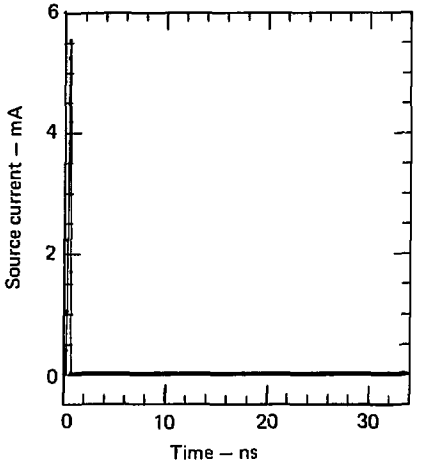

Fig. 34. The transient feedpoint current.

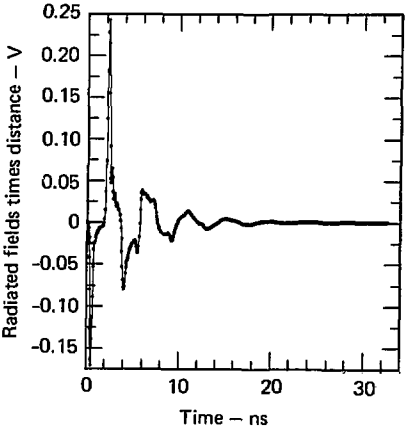

Fig. 35. The radiated field possesses a fundamental frequency twice that of an unloaded dipole.

Time Gating

Time gating can be used in transient-electromagnetic measurements to eliminate the effects of reflections from scatterers physically separated from the target. This powerful technique, described above, provides wideband information without expensive anechoic chambers, etc. But time gating can also be used numerically, as demonstrated in Figs. 36 and 37.[47] Here, a dipole of finite length is illuminated by the time derivative of a Gaussian plane wave at broadside incidence. Figure 36 shows the current at the center of the dipole. The calculation ended before end reflections arrived. Thus, time gating permits us to obtain an infinite-wire response from a finite-wire response. Transformation to the frequency domain establishes the validity of this approach for the transfer admittance. Figure 37 shows the analytic results and the FFT of Fig. 36. We can find the frequency range over which this technique produces valid data in the same way as in transient measurements. The clear time determines the lowest frequency of valid data, and the sampling requirements determine the highest frequency.

Time gating can also be used to study the propagation of a current pulse along a wire, reflections from ends of wires, reflections from junctions of wires, and similar phenomena. Judicious use of existing codes can accomplish all these results; no modifications are required.

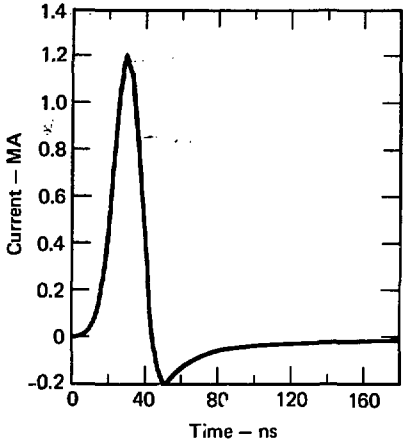

Fig. 36. Time-range gating can be used to separate reflection effects from other phenomena. In this example, the computed current on a long (120 m) center-fed dipole modeled with 120 segments prior to end reflection is extrapolated in time to approximate the current that would be seen on an infinite antenna.

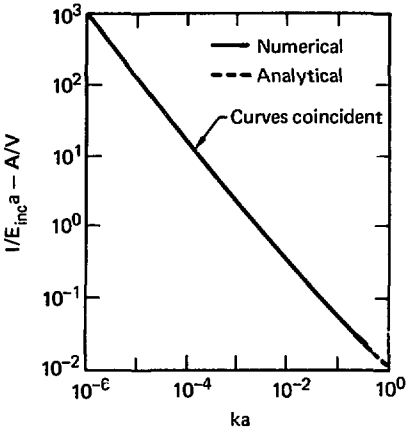

Fig. 37. The transfer function can be obtained by transforming the current from Fig. 36 to the frequency domain. The transfer function compares well with analytical results. Several calculations were required to span the ka range shown.[47]

AREAS OF APPLICATION

The following list of examples show fairly comprehensively the potential of direct time-domain techniques. Applications demonstrated by previous results are referred to but not repeated.

Antenna Characteristics

Time-domain techniques can directly evaluate the transient characteristics of antennas. Driving-point currents (Figs. 10, 22, 34), radiated far fields (Figs. 2, 35), and near fields may be found. Transformation to the frequency domain produces antenna driving-point characteristics (Figs. 11, 23) and the antenna gain (Figs. 12, 25).

Scatterer Characteristics

Direct time-domain analysis conveniently provides the receiving and scattering properties of metallic objects. It also provides antenna effective heights (Fig. 19) and monostatic or bistatic radar cross sections (Fig. 20).

Transient Response

Another obvious application of transient analysis is the calculation of coupling such as that due to EMP. These techniques can be used straightforwardly to obtain EMP responses. For example, in Figs. 30-32 we showed the response of a 10-m straight wire illuminated from broadside by an EMP pulse. We can use such calculations directly as obtained or can compare them with step responses, etc. to assess the importance of detail in the incident waveform. The ease of obtaining these responses conveniently permits efficient parameter studies. Figures 38 and 39 shows the results of one such study. Here, wires of different lengths were exposed to an EMP pulse. The wires were loaded resistively at their centers, and the value of resistance was also considered a parameter. For each combination of length and resistance, the transient calculation was performed and the peak load current and total load energy evaluated. Figures 38 and 39 present the results of these calculations as contour plots, where the loci describe parameter pairs that produce the same peak current on total energy. Such plots are invaluable for condensing and evaluating large amounts of data. These plots show, for example, that peak current is approximately proportional to wire length in the wire-length range from several meters to several hundred meters. Resistive loading of several ohms to several hundred ohms does not drastically affect peak currents or total energy. Calculations for reactive loads show that a single resistance in series with a resistance has little effect on total energy collected.

EMC and RFI Analysis

In general, EMC and RFI predictions need the electromagnetic characteristics of objects over a wide bandwidth. Transient methods provide such information efficiently. The potential of this application was demonstrated previously with the transfer function for reception of the conical spiral (Figs. 18, 26) and similar calculations.

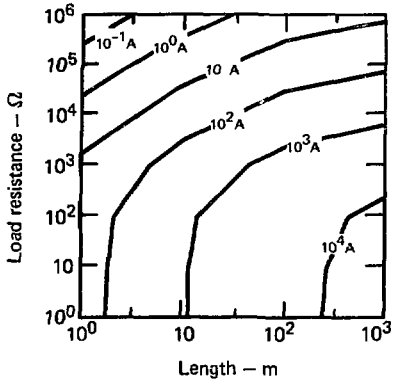

Fig. 38. The value of a time-domain computation in finding an efficient early-time solution. Here, the peak current excited on a dipole by a broadside-incident EMP pulse (see Fig. 30) is plotted as a constant contour value as a function of wire length (m) and center load-resistance value (ohms). The time-domain computation permits the peak current, which occurs early in time, to be found without requiring a complete transient waveform.

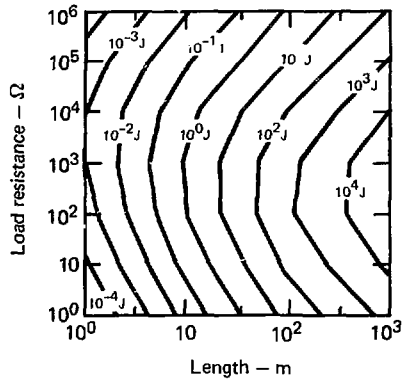

Fig. 39. Total load energy plotted as a constant contour value as a function of wire length (m) and center load-resistance value (ohms). The energy calculation requires that I^2R decay to a small value before terminating the calculation.

First-Look Studies

Transient methods can also be used effectively for preliminary analysis of new antenna structures. Such studies provide information on antenna bandwidth and input and receiving characteristics. This approach was used to develop an antenna for an implantable transponder.[48] The characteristics of a candidate bow-tie antenna depicted in Fig. 40 are shown in Figs. 41 and 42 This geometry was subsequently used. Antenna characteristics sought were broad bandwidth and large effective height. The candidate shown here was chosen over arrays of dipoles, loops, and several other types of antennas because of its acceptable performance, simple construction, and packaging ease. Antenna design using numerical techniques provided insight almost impossible to obtain experimentally with available equipment and time.

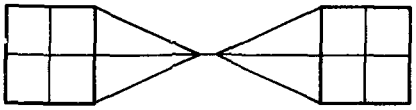

Fig. 40. Bow-tie antenna developed as part of an implantable transponder for animal monitoring. The final design was selected on the basis of efficiency, bandwidth, and impedance.

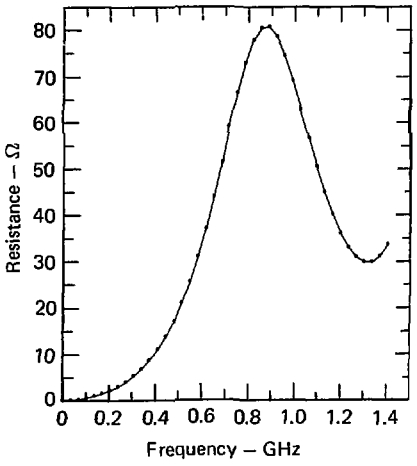

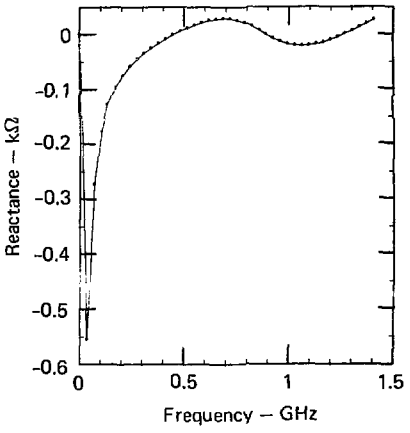

Fig. 41. Frequency-domain results of time-domain computation.[48]

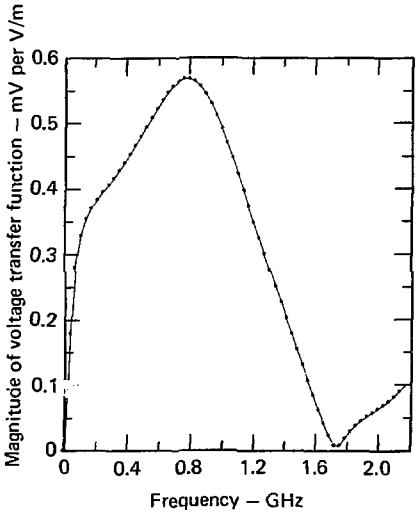

Fig. 42. Additional frequency-domain results of time-domain computation.

Assessment of Transient-Measurement Performance

Numerical transient techniques are invaluable in assessing the performance of a transient measurement facility and conversely. Comparison of measured and computed results can validate range calibration. Figure 9 shows the calculated and measured current at the base of a V-dipole over a perfect ground plane. These calculations used the actual applied voltage and modeled the transmitting wire as well as the target. It must be emphasized that no normalization or other operation was performed on the data shown in Fig. 9; they are presented directly as measured and calculated. This plot illustrates that the magnitude of the measurements is well calibrated but that the time base is slightly in error.

Transient techniques can be used in other ways to assess the performance of the transient-measurement facility. For example, the source antenna radiates primarily from the point where the antenna is fed at the ground plane. Such radiation produces a spherical wavefront. Figures 43 and 44 compare the spherical-wave response of various-length dipoles to that of dipoles illuminated by a plane wave. As one would expect, the differences between plane-wave and spherical-wave excitation are small as long as the target is small with respect to the radius of curvature of the wavefront. This result allows one to place quantitative limits on target size.

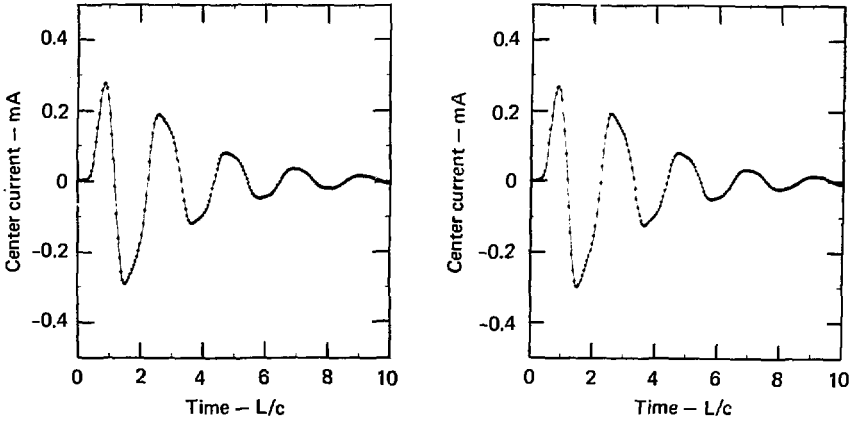

Fig. 43. Transient-range application of time-domain computation. The effect of radiating-source proximity to a straight wire was studied with respect to the wire's response to plane-wave excitation, using a Gaussian pulse. Here, distance of the point source is 1.5 m and wire length is 0.4 m.

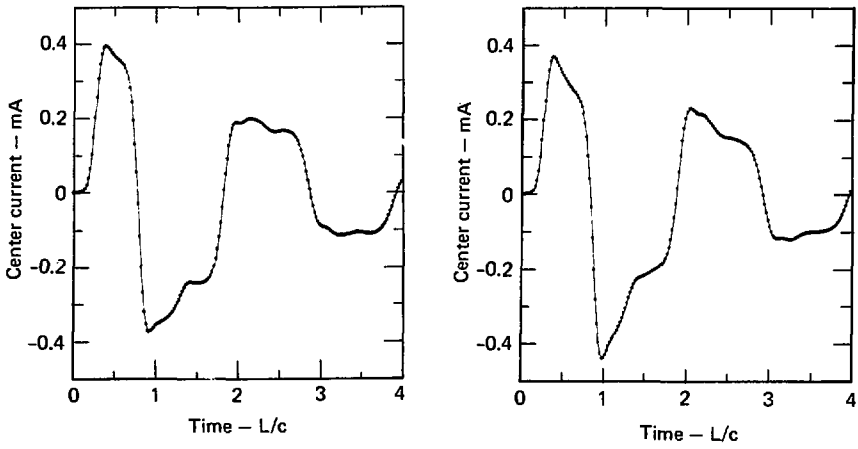

Fig. 44. Here, distance of the point source is 1.5 m and wire length is 1 m. In this case, there is a discernible difference between the plane-wave and point-source-induced current.

Study of Modeling Errors

We may identify two essentially independent error types associated with a computation. One arises from replacing the actual physical object of interest by an idealized numerical model. This error can be characterized as a physical modeling error, which we denote by ε_p. The other arises in obtaining a numerical solution for the idealized model. We refer to this error as a numerical modeling error and denote it by ε_N. One way to assess both errors is to perform measurements on the actual and idealized object to establish ε_p, and to compare measured and calculated results for the idealized model to determine ε_N.

In Figs. 45-47 we present results from measurement and computation performed for this purpose. The measured curves obtained on the LLL transient range (Fig. (46)) pertain to a scale-model 747 aircraft and a pipe and thin-wire approximation (Fig. 45) when the models are mounted nose down and perpendicular to a ground plane, the point at which the current was measured. These curves are similar in shape for the first portions of the waveforms, except for an amplitude difference which can be attributed to their different cross-sectional size. The later parts of the waveforms do not agree as closely, revealing the effects of model differences on the induced current.

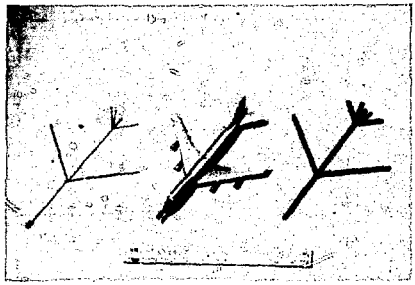

Fig. 45. Physical and numerical modeling errors can be assessed using data like that in Figs. 45-47.[32] Here, measured responses of a scale-model and pipe and thin-wire models of a 747 aircraft are shown.

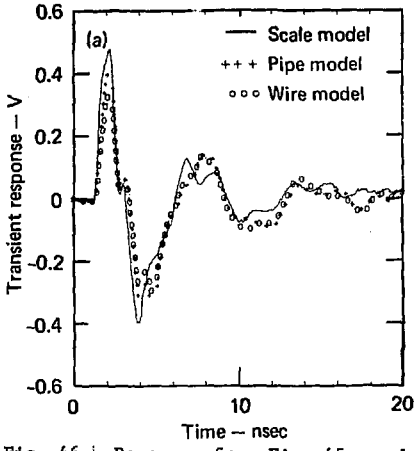

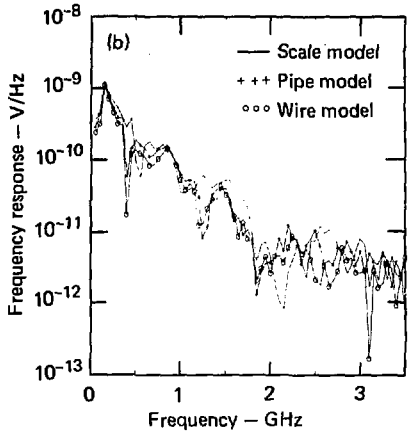

Fig. 46. Response from Fig. 45 can be used to evaluate the physical modeling error.

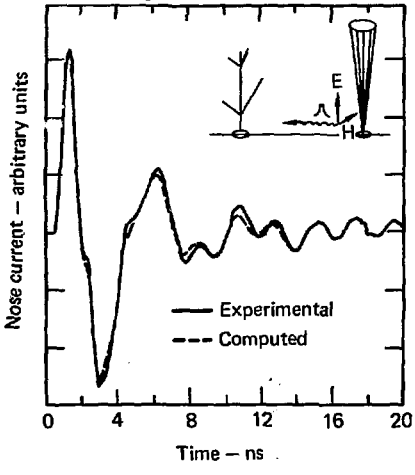

Fig. 47. The numerical modeling error can be examined by comparing measured and computed results for the numerical model. In general, as observed here, the numerical error will be less than the physical error.

The computed and measured curves for the pipe model (Fig. 47), by contrast, track very closely over the entire waveforms shown. This result increases our confidence in using the time-domain computation for somewhat more complex objects. Overall, we can also decide whether the physical modeling error revealed by the measurements may be acceptable for the intended application, although this decision may hinge on obtaining further data (e.g., scattered fields) or presenting it in a different format (e.g., as a transfer function).

Object-Pole Finding

Prony's method is a curve-fitting scheme that fits Eq. (1) to transient measured or calculated data by computing values for R_α and s_α.

The pole locations are independent of the temporal or spatial nature of the excitation. This means that one need not employ any special excitations; the only requirement is that the excitation band span the poles of interest. The orientation of the scatterer is also immaterial, so that the same resonance locations are obtained whatever the angle of incidence or polarization. In some special cases, however, some resonances may be absent. Figures 48 and 49 illustrate application of the Prony technique. Figure 48a shows the backscattered field from a dipole 60 meters long for an incident Gaussian field 30° from broadside, and Fig. 49a shows the resulting pole locations. Figures 48b and 49b show the results of repeating these calculations for 60° (from broadside) incidence. Although the temporal nature of the scattered field has changed, the pole locations have not.

Figures 50 and 51 show results of resistively loading the dipole at its center, and bending it at a right angle at its center. In the former case, the α = 1, 3, 5, ... poles are more lossy than the α = 2, 4, 6, ... poles, while the converse is true in the latter case. This occurs because the odd-numbered modes are even about the dipole's center, so that the resulting current maxima at the resistive loads produce a large dissipative loss, while the even-numbered modes are odd and have charge maxima at the center, thus producing a large radiative loss at the bend.

Besides being useful to find the pole locations for SEM, Prony's method serves as well to store the transient waveform in a shorthand form. One interesting application of data handling is the ability to extrapolate both forward and backward in time. Figure 52 shows a portion of the computed backscattered field observed from the wire object shown. Figure 53 plots the

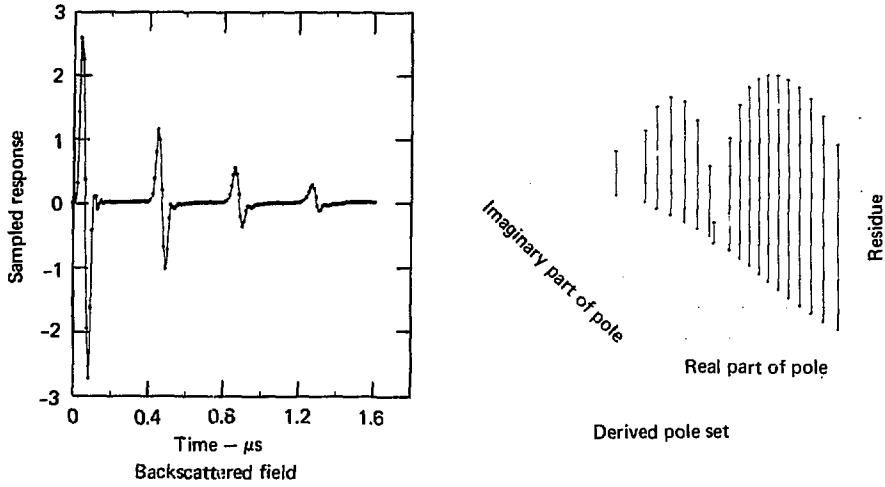

Fig. 48. SEM poles can be directly extracted from transient waveforms using Prony's method.[29,30] Results given here for the transient field scattered from a dipole illuminated by a Gaussian pulse at 30° incidence yield the pole set s_α, shown.

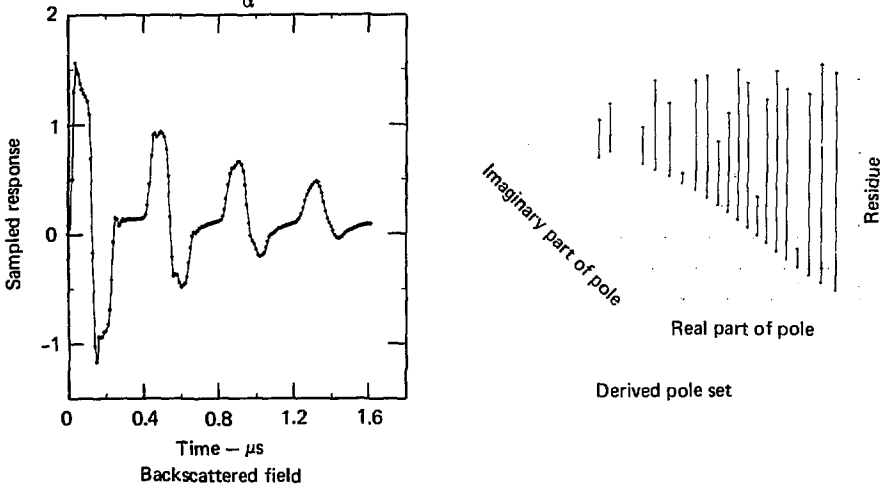

Fig. 49. Results given here for the transient field scattered from a dipole illuminated by a Gaussian pulse at 60° incidence yield the pole set, s_α, shown. Note that, in spite of the extremely different waveforms, the pole locations are the same as in Fig. 48. All the waveforms difference is due to variations in the residues, R_α, presented here in magnitude as vertical lines on a log scale.

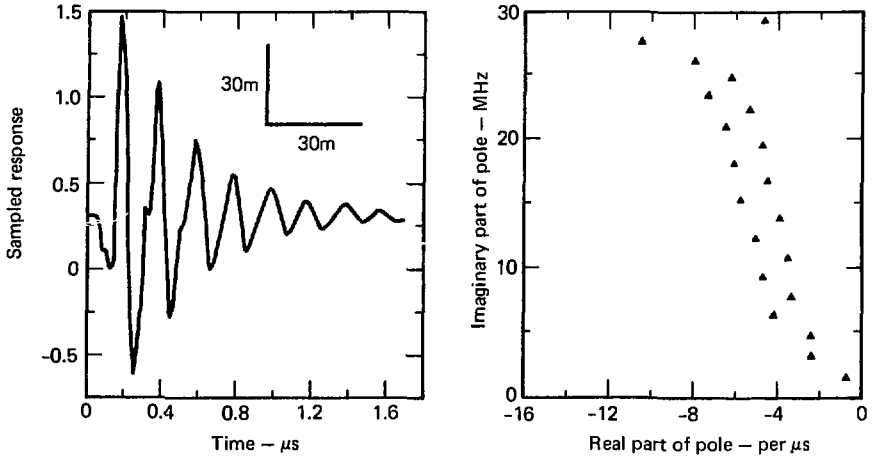

Fig. 50. Energy loss mechanisms can affect the pole locations in the complex frequency plane.[30] Here we present the pole sets for a 60-m wire, showing the result when the wire is straight and loaded with a 100-ohm resistance at its center.

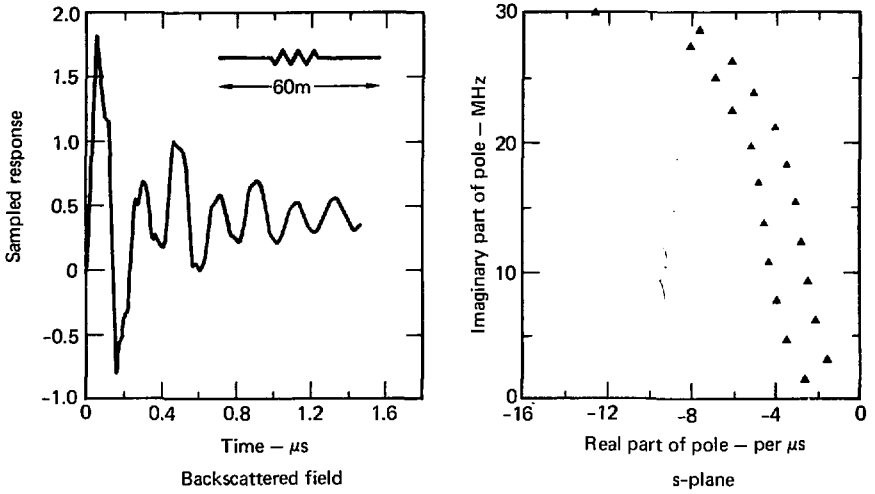

Fig. 51. Here, the wire is unloaded but has a 90° bend at its center. The $\alpha = 1, 3, \ldots$ poles are more lossy for the loaded wire, due to dissipative loss of those modes which have current maxima at its center, and the $\alpha = 2, 4, \ldots$ modes are more lossy for the bent wire, because the charge maxima at the bend produce a greater radiation loss.

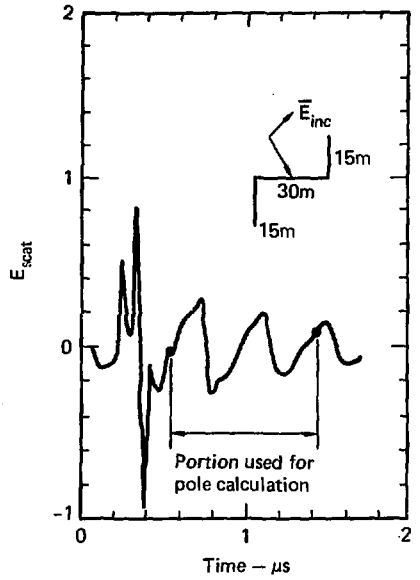

Fig. 52. Extrapolation of a transient waveform can also be accomplished using the poles extracted from it. Here, part of a computed field scattered from the thin-wire object is illustrated.

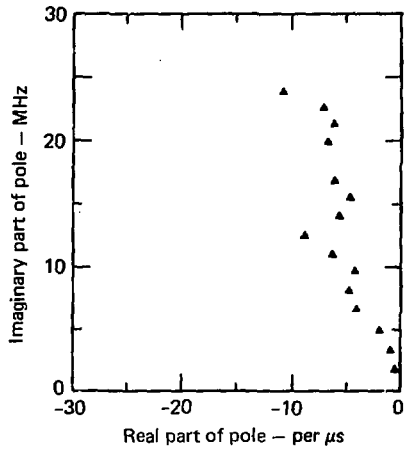

Fig. 53. Poles extracted from a portion of the transient waveform shown in Fig. 52.

pole locations obtained using only that portion of the response indicated in Fig. 52. The poles from Fig. 53 (and residues which are not shown) were then used to fill in the entire transient response. This extrapolated response is compared to the original computed response in Fig. 54, with excellent agreement.

Transient-Pulse Shaping

For some applications, it may be desired to radiate a specific transient-pulse shape. Physical constraints may prohibit the antenna from being frequency independent throughout the band of the desired pulse, and the antenna then functions as part of the wave-shaping network. Transient techniques can be used effectively in these cases to integrate the antenna's response into the design of the pulse-shaping network. For example, consider a zero-impedance voltage source connected to a conical spiral antenna (the same antenna used for the results in Figs. 22-26).[41] Assume that we want the radiated field in one polarization plane to be the third derivative of the Gaussian, i.e.,

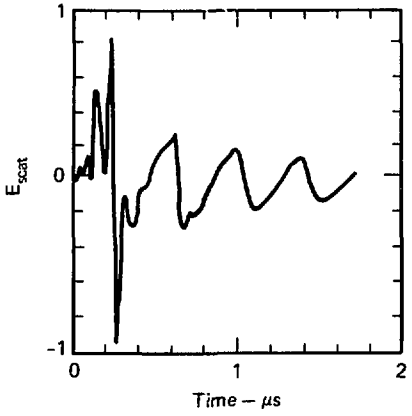

Fig. 54. The waveform reconstruction, which compares well with the original waveform both before and after the sampled portion.

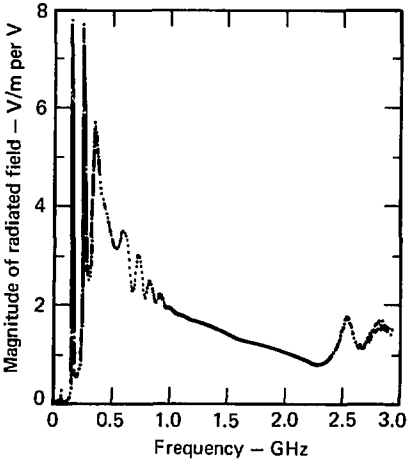

Fig. 55. Antenna pulse synthesis is straightforward using time-domain analysis.[41] Figures 55-57 illustrate one possible procedure by its application to a conical-spiral antenna (the same one considered in Fig. 22). Here we present the boresight radiation-field transfer function.

$$E_{rad}(t) \propto \frac{d^3}{dt^3} \left[(\exp(-a^2t^2)\right] \quad .$$

The desired quantity is the voltage required to be applied to the antenna to produce that far-field behavior. To find this quantity, we first calculate the transfer function between the radiated field and the applied voltage, which is shown in Fig. 55 for the conical antenna previously considered. Next, we obtain the spectrum of the required voltage by dividing the spectrum of the desired radiated field by this transfer function. The spectrum of the desired field must go to zero with decreasing frequency faster than the transfer function, because the antenna cannot radiate a static field. We then find the required transient voltage (Fig. 56) by transforming this spectrum to the time domain. To verify the result, we use this waveform in the TWTD code to obtain the radiated field shown in Fig. 57 from the direct time-domain calculation. This waveform is the desired third-time derivative of the Gaussian as specified. A similar approach could also be used with measured antenna characteristics.

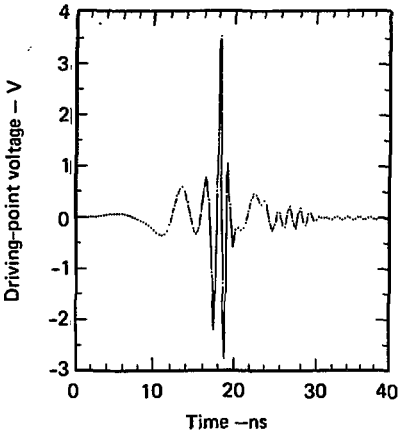

Fig. 56. The transient voltage waveform required for the antenna to radiate the third derivative of a Gaussian pulse.

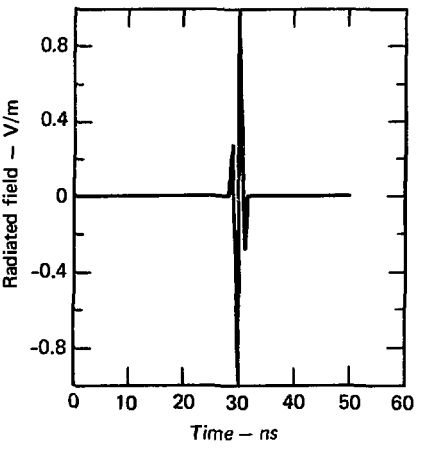

Fig. 57. The actual radiated field produced by application of the voltage pulse in Fig. 56.

Physical Insight

Transient methods can be advantageously used to help understand the characteristics of the electromagnetic response of structures. The physical insight thus made possible may be greatly enhanced by novel data-presentation techniques. For example, there are physical differences between the radiation properties of the linear dipole and conical spiral, as previously demonstrated. A motion picture of the currents along the structure as well as the radiated fields would show the differences between their radiation processes clearly. Specifically, the dipole radiates when current pulses are reflected from the ends of the dipole, while the conical spiral radiates continuously as the current pulse travels along the wire.

A motion picture format is not always suitable, of course, but the presentation continuity it provides in both space and time can be obtained in other ways. One example is presented in Figs. 58 and 59. Equal-current contours are shown on these graphs as a function of position along the wire and as a function of time. Distance (horizontal axis) and time (vertical axis) are scaled so that a pulse traveling at the velocity of light in free space describes a straight line with a slope of unity.

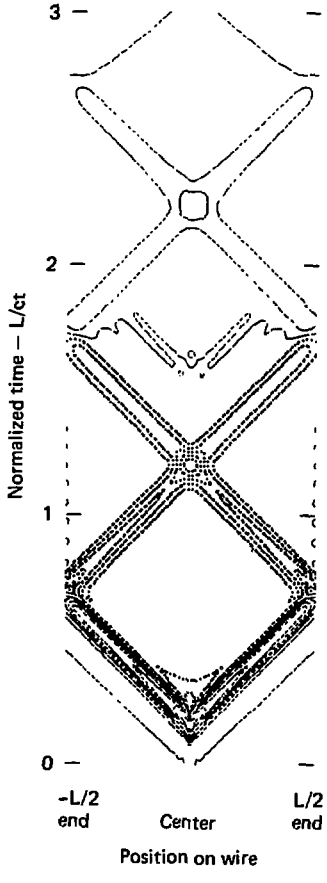

Fig. 58. Space-time contour plots of the current can convey a great deal of information concerning *transient behavior*. *Results are* presented here for a 1-m linear dipole antenna excited by a Gaussian voltage pulse. The time variation is shown on the vertical axis and the space variation is shown on the horizontal axis, where the scales are in the ratio of c, so a 45° straight line represents motion at the speed of light.

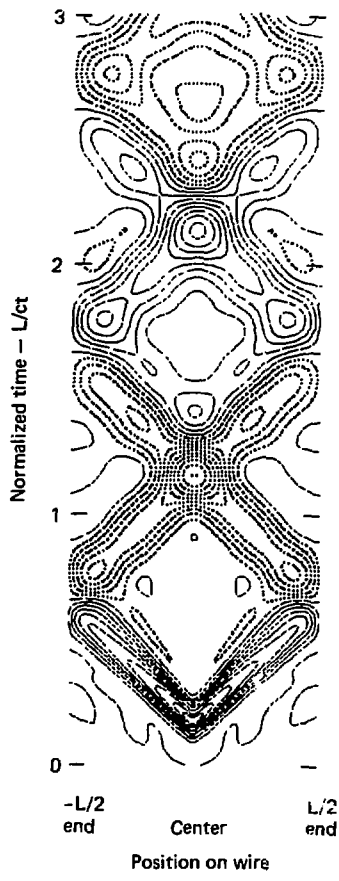

Fig. 59. Space-time contour plot of the current for a conical-spiral antenna of 1 m overall length, excited by a Gaussian voltage pulse. The difference in radiation mechanisms for the two antennas, and other features as well, can be deduced from these results, as discussed in the text.

The dipole response (Fig. 58) illustrates that the current pulse undergoes little decay as it travels along the wire, as shown by the closing of all the contours near the wire's end, but that the current pulse reflected from the ends is slightly less than that incident; energy has been lost to radiation. The current along the conical spiral (Fig. 59), however, is continually decaying as shown by closing of the contours along the entire length of the antenna. The explanation of both these responses is that accelerated charge provides the radiation. This also explains why the dipole produces linear polarization and why the conical spiral produces circular polarization. Also observe that the current contours on the straight wire are parallel, showing that leading and trailing edges of the pulse propagate with little dispersion. By contrast, the pulse on the spiral broadens due to dispersion, as shown by the nonparallel current contours.

Exciting the object as a scatterer provides comparable insight. Again, novel data presentation, such as film strip, contour plots, etc., quickly permit one to sense a structure's response. For example, the analytic frequency-domain solution of an infinite cylinder provides an approximate low-frequency transfer function between incident field and excited current as $1/i\omega$. This implies an integral relationship; i.e., the current is approximated by a constant times the integral of the electric field. Transient analysis indeed verifies this fact,[47] as mentioned earlier in the section dealing with time gating. Transient analysis also shows that the integral relationship holds everywhere on the wire until the effects of the ends of the wire are observed. Such knowledge permits easy prediction of peak currents for step-like or pulse-like excitations[49] and also permits easy prediction of current sensitivity to incident field parameters such as rise time, fall time, and peak field strength.

Wire-Grid Models

Wire grids or meshes are frequently used to approximate solid or closed-surface objects because of the computational convenience they provide. One example of a rather simple wire-grid model is provided in Figs. 60 and 61, where the computer model for a 747 aircraft is shown in Fig. 60. The total axial current induced on this model by a broadside incident EMP is given in Fig. 61 as calculated at a point just behind the wing. The induced peak current of about 6800 amp agrees reasonably well with the value indicated by

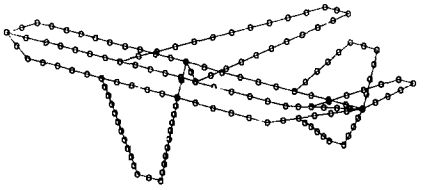

Fig. 60. Simple wire-grid model of 747 aircraft.

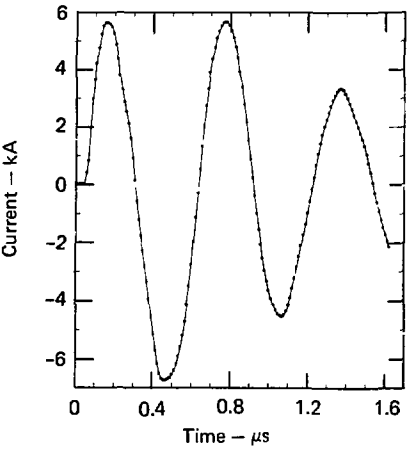

Fig. 61. Wire-grid model of 747 was used to obtain the total axial current flow on the fuselage immediately behind the wings. This result was obtained for a broadside-incident nominal EMP and agrees well with other results for a simple stick model in terms of the peak current.

Fig. 38 for a wire of length ~70 m, the difference arising because of their different radii.

A more complicated grid problem is depicted in Fig. 62 of a wire-grid model of a light truck with a rear-mounted 108-inch whip antenna. The effect of the ground was included as a perfect image plane. Figure 63 show the results for the imput admittance obtained from a time-domain calculation. An input resistance of ~70 ohms occurs at 27 MHz, the operating frequency of the transmitter, which may be recognized as the CB frequency. This result has been verified by actual operation, demonstrating the utility of the wire-grid model.

A variety of other wire-grid calculations have also been performed using the time-domain approach. These include mesh models for plates, a fan-type antenna, and a conical shell. Because wire grids are only physical approximations to closed surfaces, care must be exercised in their use, however.

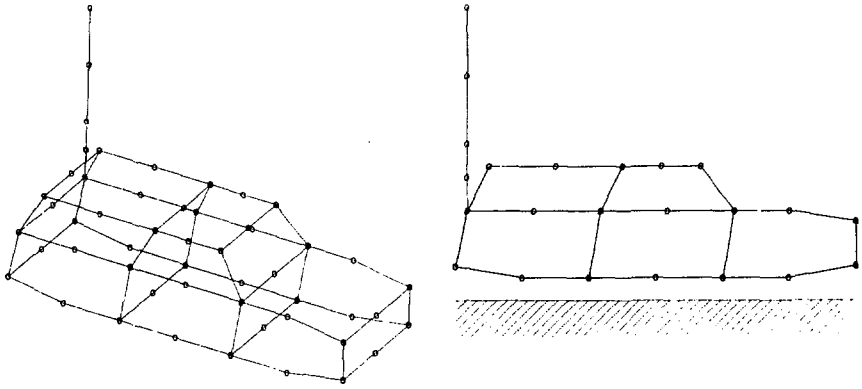

Fig. 62. Wire-grid model of a light truck located over a perfect ground plane, used to compute the impedance characteristics of a 108-inch whip antenna mounted as shown.

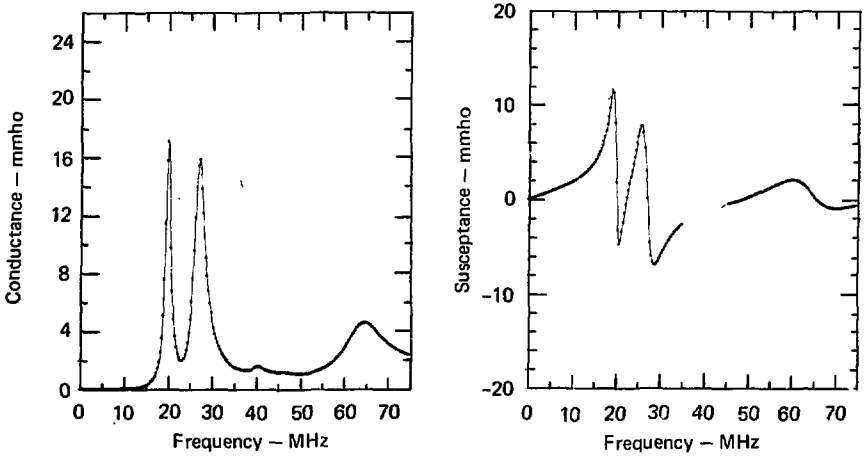

Fig. 63. The antenna admittance demonstrates an input impedance of ~70 ohms at 27 MHz, the frequency of operation for this emergency communication system (CB radio).

Conclusion

In this report, we have tried to present the rudiments of EM transient analysis via the use of direct time-domain integral-equation solutions, and to demonstrate their utility for a variety of applications. We have emphasized the physical aspects of transient behavior and examined the numerical treatment in some depth, while introducing a minimum of mathematical detail. The single most important point we would like to leave with the reader is an appreciation for the practical utility of direct time-domain techniques in providing greater insight and understanding of electromagnetic phenomena. Direct techniques also offer greater solution efficiency than transform techniques for many types of transient problems, the ability to handle nonlinearities, the convenience of wide-bandwidth information from a single calculation, the opportunity to use time-range gating to isolate interactions, and the possibility for directly obtaining the complex resonances of objects excited by EM sources. In closing, we hope the reader will be encouraged to employ transient computation and measurement where appropriate as an additional tool for solving EM problems.

Acknowledgments

The authors appreciate the assistance of discussions they had with several colleagues while preparing this work. These colleagues include R. M. Bevensee, J. N. Brittingham, G. J. Burke, F. J. Deadrick, T. Lehman, and A. J. Poggio. They are also grateful to M. Schmidt and P. Lorton for their skill and diligence in typing the manuscript, and to Robert Waite for his patience and care in editing it.

References

1. E. K. Miller, *Some Computational Aspects of Transient Electromagnetics*, Lawrence Livermore Laboratory, Livermore, Calif., UCRL-51276 (1972).
2. A. J. Poggio and E. K. Miller, "Integral Equation Solutions of Three-Dimensional Scattering Problems," in *Computer Techniques for Electromagnetics*, R. Mittra, Ed. (Pergamon Press, New York, 1973), Ch. IV.
3. G. Franceschetti and C. H. Pappas, "Pulsed Antennas," *IEEE Trans. AP-S*, 22 (5), 651 (1974).
4. L. Felsen, Ed., *Transient Electromagnetics* (Springer-Verlag, New York, 1976).
5. E. K. Miller, J. A. Landt, and A. J. Poggio, *Electromagnetic Transient Radiation and Scattering* (University of California Press, Berkeley, Calif., 1977).
6. P. O. Brundell, "Transient Electromagnetic Waves around a Cylindrical Transmitting Antenna," *Ericsson Tech.* 16 (1), 137-162 (1960).
7. O. Einarsson, "The Step-Voltage Current Response of an Infinite Conducting Cylinder," *Trans. Roy. Inst. Technol. Stockholm* 191 (1962).
8. F. J. Friedlaender, *Sound Pulses* (Cambridge University Press, London, 1958).
9. I. Rheinstein, "Backscatter from Spheres: A Short Pulse View," *IEEE Trans. Ant. and Prop.* 16, 89 (1968).
10. C. Flammer and H. E. Singhaus, "The Interaction of Electromagnetic Pulses with an Infinitely Long, Conducting Cylinder above a Perfectly Conducting Ground," *AFWL Interaction Note* 144 (1973).
11. P. R. Barnes and D. B. Nelson, "Transient Response of Low Frequency Vertical Antennas to High Altitude Nuclear Electromagnetic Pulse (EMP)," *AFWL Interaction Note* 160 (1974).
12. E. M. Kennaugh and D. L. Moffatt, "On the Axial Echo Area of the Cone Sphere Shape," *Proc. IRE (Correspondence)* 50, 199 (1962).
13. E. M. Kennaugh and D. L. Moffatt, "Transient and Impulse Response Approximations," *Proc. IEEE* 53, 893 (1965).
14. C. L. Bennett and W. L. Weeks, *Electromagnetic Pulse Response of Cylindrical Scatterers," G-AP Symposium, Boston, Mass., 1968.* See also *A Technique for Computing Approximate Electromagnetic Impulse Response of Conducting Bodies*, Purdue University, Lafayette, Ind., Report TR-EE68-11.

15. E. P. Sayre, *Transient Response of Wire Antennas and Scatterers*, Electrical Engineering Department, Syracuse University, Syracuse, N.Y., Technical Report TR-69-4 (1969).

16. C. L. Bennett and W. L. Weeks, "Transient Scattering from Conducting Cylinders," *IEEE Trans. Ant. and Prop.* 18 (5), 627-633 (1970).

17. E. P. Sayre and R. F. Harrington, "Time-Domain Radiation and Scattering by Thin Wires," *Appl. Sci. Res.* 26 (6) 413-444 (1972).

18. E. K. Miller, A. J. Poggio, and G. J. Burke, "An Integro-Differential Equation Technique for the Time-Domain Analysis of Thin-Wire Structure. Part I, the Numerical Method," *J. Comput. Phys.* 12 (1), 24-48 (1972), "Part II, Numerical Results," *J. Comput. Phys.* 12 (2), 210-233 (1972).

19. A. J. Poggio, *Space-Time and Space-Frequency Domain Integral Equations*, MBA Technical Memo MB-TM-69/63 (1969).

20. T. K. Lui and K. K. Mei, "A Time-Domain Integral Equation Solution for Linear Antennas and Scatterers," *Radio Sci.* 8 (8-9), 797-804 (1973).

21. C. E. Baum, "Electromagnetic Transient Interaction with Objects with Emphasis on Finite Size Objects, and Some Aspects of Transient Pulse Production," presented at Spring URSI Meeting, Washington, D.C. (1972).

22. F. M. Tesche, "On the Analysis of Scattering and Antenna Problems Using the Singularity Expansion Technique," *IEEE Trans. Antenna Propagat.* 21, 53-62 (1973).

23. F. J. Deadrick, H. G. Hudson, E. K. Miller, J. A. Landt, and A. J. Poggio, "Object Discrimination via Pole Extraction from Transient Fields," USNC/URSI Meeting, Urbana, Ill. (1975).

24. T. T. Wu, "Transient Response of a Dipole Antenna," *J. Math. Phys.* 2 (6), 892-894 (1961).

25. K. K. Chan, L. B. Felsen, S. T. Ping, and J. Schmoys, "Diffraction of the Pulsed Field from an Arbitrarily Oriented Electric or Magnetic Dipole by a Wedge," *AFWL Sensor and Simulation Note* 202 (1973).

26. L. B. Felsen and N. Marcuvitz, *Radiation and Scattering of Waves* (Prentice-Hall, Inc., Englewood Cliffs, N.J., 1973).

27. L. Marin, "Natural Mode Representation of Transient Scattering from Rotationally Symmetric Bodies," *IEEE AP-S Trans.* 22 (2), 266 (1974).

28. K. R. Umashankar, T. H. Shumpert, and D. R. Wilton, "Scattering by a Thin-Wire Parallel to a Ground Plane Using the Singularity Expansion Method," *IEEE AP-S Trans.* 23 (2), 178 (1975).

29. M. L. Van Blaricum and R. Mittra, "A Technique for Extracting the Poles and Residues of a System Directly from Its Transient Response," *IEEE AP-S Trans.* 23 (6), 777 (1975).

30. E. K. Miller, F. J. Deadrick, H. G. Hudson, A. J. Poggio, and J. A. Landt, *Radar Target Classification Using Temporal Mode Analysis*, Lawrence Livermore Laboratory, Livermore, Calif., UCRL-51825 (1975).

31. A. M. Nicolson, C. L. Bennett, D. Lamensdorf, and L. Susman, "Applications of Time Domain Metrology to the Automation of Broad Band Measurements," *IEEE Trans. Micro. Theory and Techniques* 20 (1), 3-9 (1972).

32. R. M. Bevensee, F. J. Deadrick, E. K. Miller, and J. T. Okada, *Validation and Calibration of the LLL Transient-Electromagnetic Measurement Facility*, Lawrence Livermore Laboratory, Livermore Calif, UCRL-52225 (1977).

33. F. Rohrlick, *Classical Charged Particles* (Addison-Wesley Publishing Co., Inc., Reading, Mass., 1965).

34. W. K. H. Panofsky and M. Phillips, *Classical Electricity and Magnetism* (Addison-Wesley Publishing Co., Inc., Reading Mass., 1956).

35. C. L. Bennett, A. M. Auckenthaler, R. S. Smith, and J. D. DeLorenzo, *Space-time Integral Equation Approach to the Large Body Scattering Problem*, Rome Air Development Center, Report RADC-TR-73-70 (1973).

36. E. K. Miller, F. J. Deadrick, and J. A. Landt, *Time-Domain Analysis of Non-linear Loads*, Lawrence Livermore Laboratory, Livermore, Calif., to be published.

37. R. F. Harrington, *Field Computation by Moment Methods* (MacMillan Co., New York, 1968).

38. R. Mittra, Ed., *Numerical and Asymptotic Techniques in Electromagnetics* (Springer-Verlag, New York, 1975).

39. J. A. Landt, E. K. Miller, and M. L. Van Blaricum, *WT-MBA.LL1B: A Computer Program for the Time-Domain Response of Thin-Wire Structures*, Lawrence Livermore Laboratory, Livermore, Calif., UCRL-51585 (1974).

40. R. W. P. King, *The Theory of Linear Antennas* (Harvard University Press, Cambridge, Mass., 1956).

41. E. K. Miller and J. A. Landt, "Short Pulse Characteristics of the Conical Spiral Antenna," *IEEE AP-S Transactions* (1977).

42. D. E. Merewether, "Transient Currents Induced on a Metallic Body of Revolution by an Electromagnetic Pulse," *IEEE Trans. Electromagnetic Compatability* 13 (2), 41-44 (1971).

43. H. K. Schuman, "Time-Domain Scattering from a Non-linearly Loaded Wire," *IEEE AP-S Trans.* 22 (4), 611 (1974).

44. T. K. Liu and F. M. Tesche, "Analysis of Antennas and Scatterers with Non-linear Loads," *IEEE AP-S Trans.* 24 (2), 131 (1976).

45. T. K. Sarkar and D. D. Weiner, "Scattering Analysis of Non-linearly Loaded Antennas," *IEEE AP-S Trans.* 24 (2), 125 (1976).

46. P. P. Toulios, *Antenna User's Manual for Linear Cylindrical Antennas in an EMP Environment*, Illinois Institute of Technology Research Institute, Report on Contract No. DAAG39-72-C-0192, Project. No. IITRIE6238 (1974).

47. J. A. Landt and E. K. Miller, "Transient Response of the Infinite Cylindrical Antenna and Scatterer," *IEEE AP-S Trans.* 24 (2), 246 (1976).

48. D. M. Holm, R. E. Bobbett, A. R. Koelle, J. A. Landt, W. M. Sanders, S. W. Depp, and J. L. Seawright, "Passive Electronic Identification with Temperature Monitoring," in *Proc. on Symposium on Cow Identification Systems and Their Applications* (Wageningen, Netherlands, 1976), pp. G1-G13.

49. J. A. Landt, *Peak Current Estimates: Cylinders in Free Space with Extensions to Other Structures*, Lawrence Liverore Laboratory, Livermore, Calif., Nuclear EMP Protection Engineering and Management Note, PEM-32 (1974).

RGW/jcn/vt/lm

Appendix

The derivation of Eq. (2h) follows readily from the approach used to develop the Poynting's vector. From Maxwell's equations

$$\nabla \times \overline{E} = -\mu_0 \frac{\partial}{\partial t} \overline{H} \ , \tag{A1}$$

$$\nabla \times \overline{H} = \varepsilon_0 \frac{\partial}{\partial t} \overline{E} \ , \tag{A2}$$*

and the $\overline{H}$ • product of (A1), the $\overline{E}$ • product of (A2), and their difference, we obtain

$$\nabla \cdot \overline{E} \times \overline{H} = -\mu_0 \overline{H} \cdot \frac{\partial}{\partial t} \overline{H} + \varepsilon_0 \overline{E} \cdot \frac{\partial}{\partial t} \overline{E} \ , \tag{A3}$$

where we have used

$$\overline{A} \cdot \nabla \times \overline{B} - \overline{B} \cdot \nabla \times \overline{A} = \nabla \cdot \overline{A} \times \overline{B} \ .$$

If Eq. (A3) is integrated over a volume V that contains the conducting body, there is found

$$\int_V \nabla \cdot \overline{E} \times \overline{H} dv' = -\frac{1}{2} \int_V \frac{\partial}{\partial t} [\mu_0 \overline{H} \cdot \overline{H} + \varepsilon_0 \overline{E} \cdot \overline{E}] dv' \ . \tag{A4}$$

Upon using the Gauss divergence theorem and integrating with respect to time, we obtain

$$\int_{-\infty}^{t} dt' \oint_A \overline{E} \times \overline{H} \cdot d\overline{a}'$$

$$= -\frac{1}{2} \int_{-\infty}^{t} dt' \int_V \left[\mu_0 \frac{\partial H^2}{\partial t'} + \varepsilon_0 \frac{\partial E^2}{\partial t'} \right] dv'$$

$$= -\frac{1}{2} \int_V \left[\mu_0 H^2 + \varepsilon_0 E^2 \right] dv' \ . \tag{A5}$$

*Note that an explicit source ($\overline{J}$) term is not included since the source here is an incident electric field.

Now let the volume V be congruent with the volume (V_c) of the conductor, assumed to be a wire, and extend a distance d beyond its surface. Then in the right side of Eq. (A5), we can approximate $\overline{H}$ and $\overline{E}$ by

$$\overline{H} \approx \overline{I}/2\pi r = \hat{s}I/2\pi a \tag{A6a}$$

$$\overline{E} \approx \hat{n}Q/2\pi r\varepsilon_0 \quad , \tag{A6b}$$

since $\hat{n} \cdot \overline{H} \approx 0$ and $\hat{s} \cdot \overline{E} \approx 0$ in the space between V and V_c. Thus, the right side of Eq. (A5) takes the form

$$RHS \approx -\frac{1}{2} \int_C \int_a^{d+a} \int_0^{2\pi} \left[\mu_0 \frac{I^2}{(2\pi r)^2} + \varepsilon_0 \frac{Q^2}{(2\pi r \varepsilon_0)^2} \right] dw' dr' r' d\phi' \quad , \tag{A7}$$

where C is the wire contour and we have neglected the contributions to the volume integral of its ends (if the wire is open ended). When the r' and ϕ' integrals of Eq. (A7) are performed, we finally obtain

$$\approx -\frac{1}{4\pi} \log\left(\frac{d+a}{a}\right) \int_C \left(\mu_0 I^2 + {}^2/\varepsilon_0 \right) dw' \quad , \tag{A8}$$

which gives rise to Eq. (2h).

The left side of Eq. (A5) can be similarly simplified to obtain

$$LHS \approx \int_{-\infty}^{t} dt' \int_C \overline{E} \cdot \overline{I} dw' \quad . \tag{A9}$$

Because $\overline{E} \cdot \overline{I} = E_{tan} I = (E_{inc} + E_{scat}) \tan I = 0$ on a perfect conductor, Eq. (2f) for the collected energy immediately follows. When there is loss on the conductor, then $E_{tan} I = E_{loss} I = (IR)I$, from which Eq. (2g) also follows.

G. P. O. 789-086/4913